

Generative Capacity of Probabilistic Protein Sequence Models

Francisco McGee^{1,2,4}, Quentin Novinger^{2,5}, Ronald M Levy^{1,3,4,6}, Vincenzo Carnevale^{2,3,*}, and Allan Haldane^{1,6,*}

¹Center for Biophysics and Computational Biology, Temple University, Philadelphia, 19122, USA

²Institute for Computational Molecular Science, Temple University, Philadelphia, 19122, USA

³Department of Biology, Temple University, Philadelphia, 19122, USA

⁴Department of Chemistry, Temple University, Philadelphia, 19122, USA

⁵Department of Computer & Information Sciences, Temple University, Philadelphia, 19122, USA

⁶Department of Physics, Temple University, Philadelphia, 19122, USA

*Corresponding authors: vincenzo.carnevale@temple.edu, allan.haldane@temple.edu

ABSTRACT

Variational autoencoders (VAEs) have recently gained popularity as generative protein sequence models (GPSMs) to explore fitness landscapes and predict the effect of mutations. Despite encouraging results, a quantitative characterization of the VAE-generated probability distribution is still lacking. In particular, it is currently unclear whether or not VAEs can faithfully reproduce the complex multi-residue mutation patterns observed in natural sequences arising due to epistasis. In other words, are frequently observed subsequences assigned a correspondingly large probability by the VAE? Using a set of sequence statistics we comparatively assess the accuracy, or “generative capacity”, of three GPSMs: a pairwise Potts Hamiltonian, a vanilla VAE, and a site-independent model, using natural and synthetic datasets. We show that the vanilla VAE’s generative capacity lies between the pairwise Potts and site-independent models. Importantly, our work measures GPSM generative capacity in terms of higher-order sequence covariation and provides a new framework for evaluating and interpreting GPSM accuracy that emphasizes the role of epistasis.

Introduction

Recent progress in decoding the patterns of mutations in protein multiple sequence alignments (MSAs) has highlighted the importance of mutational covariation in determining protein function, conformation and evolution, and has found practical applications in protein design, drug design, drug resistance prediction, and classification.¹⁻³ These developments were sparked by the recognition that the pairwise covariation of mutations observed in large MSAs of evolutionarily diverged sequences belonging to a common protein family can be used to fit maximum entropy “Potts” statistical models.⁴⁻⁶ These contain pairwise statistical interaction parameters reflecting epistasis⁷ between pairs of positions. These models have been shown to accurately predict physical contacts in protein structure,^{6,8-10} and have been used to significantly improve the prediction of the fitness effect of mutations to a sequence compared to site-independent sequence variation models which do not account for covariation.^{11,12} These models are “generative” in the sense that they define the probability, $p(S)$, that a protein sequence S results from the evolutionary process. Intriguingly, the probability distribution $p(S)$ can be used to sample unobserved, and yet viable, artificial sequences. In practice, the model distribution $p(S)$ depends on parameters that are found by maximizing a suitably defined likelihood function on the observations provided by the MSA of a target protein family. As long as the model is well specified and generalizes well from the training MSA, it can then be used to generate new sequences, and thus a new MSA whose statistics should match those of the original target protein family. We refer to probabilistic models that create new protein sequences in this way as generative protein sequence models (GPSMs).

The fact that Potts maximum entropy models are limited to pairwise epistatic interaction terms and have a simple functional form for $p(S)$ raises the possibility that their functional form is not flexible enough to describe the data, i.e. that the model is not well specified. While a model with only pairwise interaction terms can predict complex patterns of covariation involving three or more positions through chains of pairwise interactions, it cannot model certain triplet and higher patterns of covariation which require a model with more than pairwise interaction terms. For example, a Potts model cannot predict patterns described by an XOR or boolean parity function in

which the n -th residue is determined by whether an odd number of the $n - 1$ previous residues have a certain value (see Supplement). While some evidence has suggested that in the case of protein sequence data the pairwise model is sufficient and necessary to model sequence variation,^{13–15} some of this evidence is based on averaged properties, and there appears to be some weak evidence for the possibility of rare “higher-order epistasis” affecting protein evolution,^{7,16–18} by which we mean the possibility that subsequence frequencies of three or more positions cannot be reproduced by a model with only pairwise interactions. Fitting maximum entropy models with all triplet interactions is not feasible without significant algorithmic innovation, since for a protein of length 100 it would require approximately 10B parameters and enormous MSA datasets to overcome finite sampling error (see Supplement). However, recent developments in powerful machine learning techniques applied to images, language, and other data have shown how complex distributions $p(S)$ can be fit with models using more manageable parameter set sizes. Building on the demonstrated power of incorporating pairwise epistasis into protein sequence models, this has motivated investigation of machine learning strategies for generative modelling of protein sequence variation which can go beyond pairwise interactions, including Restricted Boltzmann Machines (RBMs),³ variational autoencoders (VAEs),^{19–22} General Adversarial Networks (GANs),²³ transformers,^{24–27} and others.

One technique in particular, the VAE,^{28,29} has been cited as being well suited for modelling protein sequence covariation, with the potential to detect higher order epistasis.^{19,20} The VAE also potentially gives additional insights into the topology of protein sequence space through examination of the “latent” (hidden) parameters of the model, which have been suggested to be related to protein sequence phylogenetic relationships.^{19–21,26} One implementation of a VAE-GPSM, “DeepSequence”, found that the VAE model was better able to predict experimental measurements of the effect of point mutations than a pairwise Potts model, which was attributed to the VAE’s ability to model higher-order epistasis.^{11,19} However, it has also been suggested by others that the improvement shown by DeepSequence could be attributed to the use of biologically motivated priors and engineering efforts, rather than because it truly captured higher-order epistasis.²⁰ Furthermore, while VAE-GPSMs are generative and aim to capture the protein sequence distribution $p(S)$, to our knowledge none of these studies have thoroughly tested what we will call the “generative capacity”^{30,31} of the VAE model, meaning the ability of the model to generate new sequences drawn from the model distribution $p(S)$, which are statistically indistinguishable from those of a given “target” protein family. Testing the generative capacity, specifically higher-order covariation, of a GPSM is a fundamental check of whether the model is well specified and generalizes well from the training set, two prerequisites to capturing higher-order epistasis.

Here, we perform a series of numerical experiments that comparatively explore the generative capacity of GPSMs. These GPSMs include a pairwise Potts Hamiltonian model with pairwise interaction terms (Mi3),³² a vanilla variational autoencoder (vVAE), and a site-independent model which does not model covariation (Indep). We choose the simplest, original^{28,29} “vanilla”³³ architecture qualitatively similar to that used in previous VAE-GPSM studies,²¹ as opposed to more complex VAE-GPSM architectures used by others (see Methods).^{19,22} We evaluate the generative capacity of a model using four MSA statistics: pairwise covariance correlations,^{2,13,34,35} higher-order marginals (r_{20}),¹³ Hamming distance distributions,^{2,13,36,37} and statistical energy correlations.¹³ We compute these statistics for MSAs generated by each GPSM, and validate the GPSMs by comparison to expectation. We also test how each GPSM behaves as fewer training sequences are provided, and thus how well the GPSMs generalize, using two training MSA sizes: one representing the estimated size upper bound for a Pfam protein family (10K) (see Supplement),³⁸ and one being large enough to eliminate out-of-sample error in our generative capacity measurements (see Results).³⁹ We evaluate GPSM performance both for natural datasets and for synthetic datasets in which the ground truth is known. Our comparative analysis thus consists of four intersecting variables: three GPSMs, a suite of four generative capacity metrics, two training MSA sizes, and two dataset types.

Our results show that while the vVAE models some epistasis, it is unable to reproduce MSA statistics as well as Mi3, but is more accurate than Indep for all metrics tested. We find that vVAE performs more similarly to Mi3 than it does to Indep according to commonly used metrics such as the Hamming distance distribution, but performs more like the Indep model for the r_{20} metric, which is the metric which most directly tests the GPSM’s ability to model higher-order sequence covariation. This result suggests r_{20} is a more sensitive measure of GPSM generative capacity than the other standard metrics. Our work consolidates several benchmark statistics of generative capacity for GPSMs, offering a novel framework for evaluating and interpreting GPSM accuracy in the context of higher-order covariation. By quantifying and comparing GPSM performance in this way, we hope to better understand the challenges and limitations inherent to generative modelling of natural protein sequence datasets, better gauge the state of the art in the field, and provide insight for future efforts in terms of minimizing the confounding effects of data limitations.

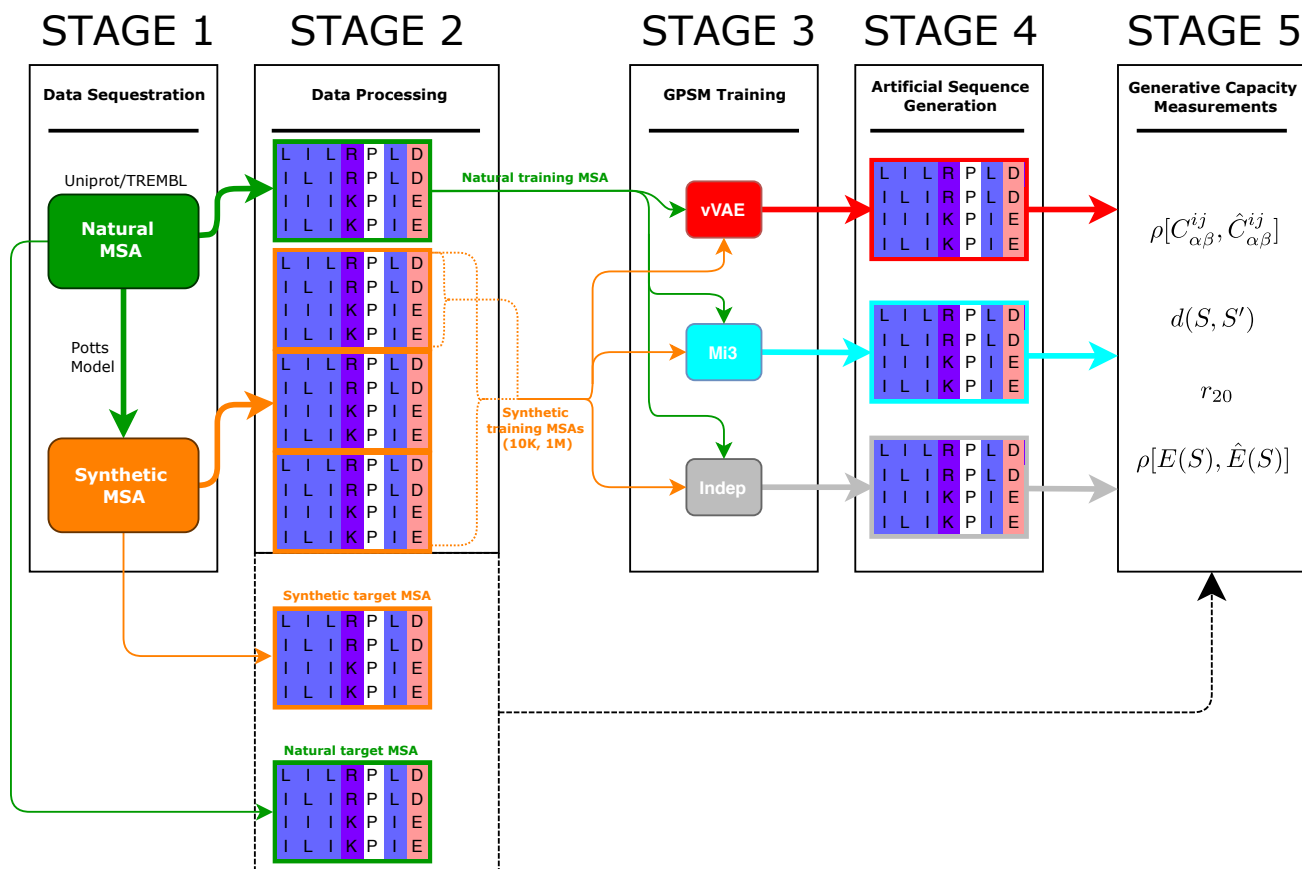


Figure 1. 5-stage analysis pipeline diagram. Stage 1: Data Sequstration. Two different MSAs are sequestered, one natural and the other synthetic, generated by a Potts model fit to the natural MSA. Stage 2: Data Processing. Sequences are indexed and split. Non-overlapping training, target, and evaluation MSAs are shown. Stage 3: GPSM Training. GPSMs are trained. Stage 4: Artificial Sequence Generation. Artificial evaluation MSAs are generated from each GPSM. Stage 5: Generative Capacity Measurements. Computation and visualization of generative capacity metrics is performed.

Results

Target Distributions

Our goal is to set baseline expectations for the generative capacity of the VAE and other GPSMs when fit to synthetic or natural protein sequence data of varying training MSA sizes. Generative models of protein MSAs define a distribution $p_{\theta}(S)$ for the probability of a sequence S appearing in an MSA dataset given model parameters θ . The model parameters are fit by either exact or approximate maximum likelihood inference of the likelihood $\mathcal{L} = \sum_{S \in \text{MSA}} p_{\theta}(S)$ over a training MSA, using regularization techniques to prevent overfitting. The sequences in the training MSA are assumed to be identical independent samples from a “target” probability distribution $p^0(S)$, which is generally unknown.²⁸ For a model with high generative capacity, $p_{\theta}(S)$ will closely approximate $p^0(S)$.²⁰ In this study, we test the generative capacity of three such GPSMs: a pairwise Potts model (Mi3),³² a vanilla VAE (see Methods), and a site-independent model (Indep), each with a different functional form of $p_{\theta}(S)$.

It is not possible to measure the similarity of $p_{\theta}(S)$ and $p^0(S)$ directly because of the high dimensionality of sequence space, since the number of sequence probabilities to compare is equal to q^L where L is the sequence length (typically ~ 300) and q is the alphabet size (~ 21). Instead we measure how derived statistics computed from evaluation MSAs generated by the GPSM match those of MSAs drawn from the target distribution. We use four statistics relevant to quantifying protein MSAs: the pairwise Hamming distance distribution, the pairwise covariance scores, higher order marginals (r_{20}), and, when possible, the GPSM’s ability to predict $p^0(S)$ for individual sequences (see Methods).

GPSM Error

We divide our tests into two analysis tracks: one synthetic, in which we train the GPSMs on synthetic MSAs generated from a known target distribution; and one natural, in which we train the GPSMs on a representative

specification error	occurs when the functional form $p_{\theta}(S)$ of a GPSM is not flexible enough to accurately model the target distribution $p^0(S)$ for any choice of parameters θ .
out-of-sample error	occurs when a GPSM fit to a finite training dataset fails to correctly model unseen data, and is a consequence of overfitting.
estimation error	occurs due to statistical error in the MSA evaluation metrics when computed from finite evaluation and target MSAs
training MSA	MSA drawn from $p^0(S)$ used to train or parameterize a model
target MSA	MSA drawn from $p^0(S)$ used as unseen data with which to evaluate the GPSM
evaluation MSA	MSA drawn from $p_{\theta}(S)$ for a parameterized GPSM, for comparison to the target MSA

Table 1. Glossary error types and the MSA datasets we use to evaluate these errors.

natural protein family MSA, the kinase super family, sequestered from Uniprot/TrEMBL.⁴⁰ These analysis tracks are meant to probe and isolate two distinct forms of error which may cause $p_{\theta}(S)$ to deviate from $p^0(S)$ (see table 1). The first is “specification error”,⁴¹ which occurs when the functional form of $p_{\theta}(S)$ of a model is not flexible enough to accurately model the target probability distribution $p^0(S)$ for any choice of parameters. A key motivation for choosing a VAE over a Potts model is its potentially lower specification error when higher-order epistasis is present.¹⁹ Indeed, Potts models are limited to pairwise interaction terms of a particular functional form, while VAEs are not. The second form of error is “out-of-sample error”,⁴² caused by a paucity of training samples, and is the consequence of overfitting.⁴³ Even a well-specified model could fail to generalize when fit to a small training dataset, and may mis-predict $p^0(S)$ for test sequences, so it follows that increasing training datasets reduces out-of-sample error. Beyond specification and out-of-sample error, which each reflect an aspect of GPSM generalization error, there can be “estimation error” in our MSA test statistics due to the finite MSA sizes we use to estimate their values, which sets an upper bound on how well these statistics can match their target values, depending on the metric.⁴⁴ Finally, other errors may arise due to implementation limitations of the inference methods, for instance due to finite precision arithmetic or to finite sample effects when Monte Carlo methods are used.

The synthetic analysis allows us to isolate specification error because the target distribution is known exactly, and we can generate arbitrarily large training, target and evaluation datasets, thereby minimizing out-of-sample and estimation error, and leaving only specification error. We specify this synthetic target probability distribution $p^0(S)$ to be exactly the Potts model distribution we inferred based on natural protein-kinase sequence data using Mi3 in our natural analysis (see Methods).³² The artificial sequences generated from this synthetic target distribution should have statistical properties similar to real, or “natural,” protein family MSAs, albeit constrained by the fact that the Hamiltonian model used to generate the synthetic dataset is limited to pairwise epistatic interaction terms only.^{6,13,45} Whereas Indep and vVAE may still fail to model this known probability distribution in the synthetic analysis, our expectation is that Mi3 will be unaffected by specification error in the synthetic tests, since the target MSA is sampled from the same probability distribution used to carry out the inference. For each generative capacity measurement, we include two synthetic training MSAs, each generated from the target model: (i) 1M sequences, which minimizes overfitting effects and consequently out-of-sample error, thereby isolating GPSM specification error in this experiment; and (ii) 10K sequences, which illustrates the expected GPSM performance on typical datasets, as most protein families in Pfam have less than 10K independent effective sequences (see Supplement).³⁸

The natural analysis examines the performance of the models on natural sequence data, which potentially contain higher-order correlations that require a Hamiltonian model with triplet or higher-order interaction terms to capture. On this dataset, vVAE could potentially outperform Mi3, depending on the importance of higher-order epistatic terms, if present.¹⁹ However, unlike in the synthetic analysis, here we do not know *a priori* the target distribution and, most importantly, we have only limited datasets for both training and evaluation. In the natural tests, the training and target MSAs each contain $\sim 10K$ non-overlapping kinase sequences from the Uniprot/TREMBL database.

Our overall testing procedure is outlined in Fig.1 (see Methods), and the terms discussed are summarized in Table 1. Our training datasets are either a natural protein sequence dataset obtained from Uniprot/TREMBL, or a synthetic training dataset. We then fit the GPSMs to the training datasets, and generate artificial evaluation MSAs from each model. Finally, using our suite of four generative capacity metrics, we compare statistics of the evaluation MSAs to those of “target” MSAs, which contain sequences drawn from the target distributions and therefore represent our expectation.

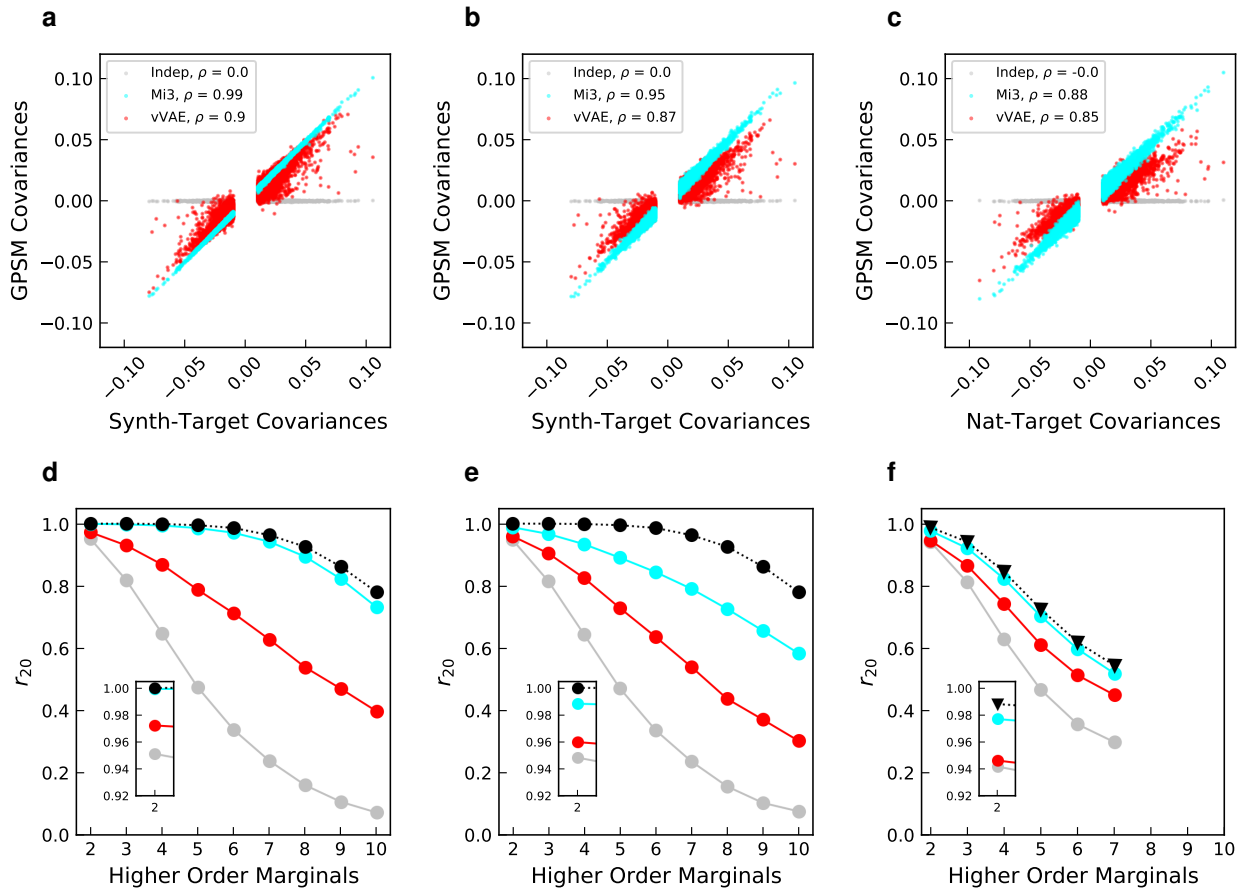


Figure 2. Pairwise covariance correlations (Top Row) and Pearson r_{20} correlations (Bottom Row). Mi3 (cyan), vVAE (red), and Indep (gray) are compared to target distribution (black, where shown). GPSMs were trained on 1M synthetic (a, d, 10K synthetic (b, e), or 10K natural (c, f) kinase sequences from the corresponding target distribution. **Top Row**, These covariance correlation plots show whether the covariances of the GPSMs match those of their respective targets at the fundamental pairwise level. Synthetic target covariances (x-axis) and artificial GPSM-generated evaluation covariances (y-axis) were computed from 500K-sequence MSAs (a, b). In contrast, due to limited availability of natural protein sequence data, natural target covariances were computed from a 10K-sequence target MSA, whereas artificial GPSM-generated covariances (y-axis) were computed from 500K-sequence evaluation MSAs (c). For each covariance scatterplot, a Pearson correlation coefficient ρ was computed between the GPSM covariance set and the target covariance set. Generative capacity for Mi3 and Indep appear insensitive to training sample size for this metric. Covariances around zero were removed for easier plotting. **Bottom Row**, These plots show whether the GPSMs, on average, have higher order marginals (HOMs) that match those of their respective targets between orders of two and ten. Insets emphasize pairwise r_{20} . Pearson r_{20} correlation (r_{20} , y-axis) is plotted as a function of HOMs (x-axis). Synthetic r_{20} were computed from 6M artificial GPSM-generated evaluation sequences compared to 6M synthetic target sequences (d, e) as colored lines, and the black dotted line here in the synthetic r_{20} analysis denotes a generative capacity upper limit set by finite sampling of two non-overlapping target MSAs of 6M sequences each. Both Mi3 and vVAE's generative capacity appear sensitive to decreasing synthetic training sample size for this metric. In contrast, for the natural analysis, the black line uses triangles to indicate a difference in how it is computed compared to the synthetic analysis (f). Here, the generative capacity upper limit is an estimate computed between non-overlapping evaluation MSAs of 6M and 10K sequences from the artificial Mi3 distribution trained on natural sequences (f, cyan), and only orders two through seven were plotted due to finite sampling effects at higher orders. In the natural analysis, Mi3 performs as close to the target as is measurable, within error, for this amount of data.

Pairwise covariance correlations

We first examine the pairwise covariance scores for pairs of amino acids of an MSA defined as $C_{\alpha\beta}^{ij} = f_{\alpha\beta}^{ij} - f_{\alpha}^i f_{\beta}^j$ where $f_{\alpha\beta}^{ij}$ are the MSA bivariate marginals, meaning the frequency of amino acid combination α, β at positions i, j in the MSA, and f_{α}^i are the univariate marginals, or amino acid frequencies at each position i . Each term measures the difference between the joint frequency for pairs of amino acids and the product of the single-site residue frequencies, i.e. the expected counts in the hypothesis of statistical independence. The scores equal 0 if the two positions do not covary. Coevolving amino acids are an important aspect of sequence variation in protein MSAs, and a GPSM's ability to reproduce the pairwise covariance scores of the training dataset has been used in the past as a fundamental, non-trivial measure of the GPSM's ability to model protein sequence covariation.^{2,13,34,35}

We compare GPSM pairwise covariance scores for all pairs of positions and residues $C_{\alpha\beta}^{ij}$ to the corresponding target pair $\hat{C}_{\alpha\beta}^{ij}$ using the Pearson correlation coefficient $\rho(\{C_{\alpha\beta}^{ij}\}, \{\hat{C}_{\alpha\beta}^{ij}\})$ (Fig. 2, Top Row). In the synthetic tests we evaluate this statistic using 500K sequences for both the target and evaluation MSAs, while for the natural test we compare 500K evaluation sequences to the available 10K target sequences. Mi3 accurately reproduces the target covariance scores in all tests ($\rho = 0.99$ in Fig. 2a, $\rho = 0.95$ in Fig. 2b, and $\rho = 0.88$ in Fig. 2c respectively). The somewhat lower value for Mi3 in the natural analysis of $\rho = 0.88$ is accounted for entirely by increased estimation error in that test as only 10K target sequences are available for evaluation, and the expected ρ due only to estimation error is $\rho \sim 0.87$ computed by comparing the natural 10K to training 10K sequences values. The high generative capacity of Mi3 is expected because Mi3 parameters are optimized to exactly reproduce the joint frequencies of pairs of amino acids from the target MSA. vVAE inference does not include this constraint, and we find that even for the largest (1M) dataset of synthetic sequences, the covariances are generally smaller in magnitude than those of the target and show smaller correlation with the target than Mi3 ($\rho = 0.9$, Fig. 2a). This amount of error in ρ can primarily be attributed to vVAE specification error, since the large training MSA of 1M sequences minimizes out-of-sample error and the large evaluation MSAs make estimation error negligible. vVAE covariances are further scaled down slightly when fit to the synthetic 10K dataset ($\rho = 0.87$, Fig. 2b). Indep cannot reproduce covariances by definition, so ρ is zero in all tests, as expected. The generative capacity trends for this metric are consistent between the synthetic and natural analyses for all GPSMs, showing the behavior is not due to artificial properties of our synthetic target model.

These results confirm that vVAE can model epistasis in protein sequence datasets, since it generates pairwise mutational covariances which are correlated with the target values, even in the absence of explicit constraints for reproducing these statistics. However, it scales down the strength of pairwise covariances in both the synthetic and natural analyses and the correlation with the target is lower than 1. Mi3, in contrast, is constrained by design to fit the covariance scores and does so nearly perfectly.

Higher order marginal statistics

A more stringent test of GPSM generative capacity is to measure the model's ability to reproduce sequence covariation involving more than two positions, or higher-order covariation. We characterize these higher-order covariation patterns in the target MSA and GPSM-generated artificial MSAs by computing the frequency of non-contiguous amino acid n -tuples, or higher-order marginals (HOMs) corresponding to subsequences, and compare their frequency in each MSA to corresponding values in the target MSAs. For increasing values of n the number of possible n -tuple combinations increases rapidly, requiring increasingly large evaluation MSAs to accurately estimate the frequency of individual n -tuples. For this reason, we limit n -tuple length to $n \leq 10$ and only compute a limited subset of all possible position sets for each n . For each n we randomly choose 3K position sets, compute the frequencies of the top twenty most frequent n -tuples for each position set in the model and target evaluation MSAs, as these are well sampled, and for each position set compute the Pearson correlation between these top twenty frequencies. We then average the correlation values for each n over all position sets. We call this metric the Pearson correlation r_{20} .¹³ In this test, estimation error is non-zero because of the extremely large MSAs required to estimate n -tuple frequencies, particularly for high $n > 5$ (see Supplement). We estimate the expected estimation error caused by finite sampling in the evaluation MSAs by computing the r_{20} scores between two non-overlapping MSAs generated by the synthetic target model, of the same size as our evaluation MSAs.

In Fig. 2, Bottom Row, we plot the HOM r_{20} for varying n . The expected estimation error (black line) represents a generative capacity upper bound, giving the highest measurable r_{20} given the evaluation MSA size of 6M for the synthetic analysis and 10K for the natural analysis. The r_{20} for Mi3 fit to 1M training sequences is very close to the validation upper-bound for all n , suggesting it has accurately fit the synthetic target distribution and its specification error is close to zero (Fig. 2d). This is expected since the synthetic target model in this test is a Potts model. With

10K training sequences, Mi3 r_{20} scores are lower than the 1M result for all n (Fig. 2e), which illustrates that Mi3 is affected by out-of-sample error for typical dataset sizes, as previously described.⁴⁵ Indep has much lower r_{20} scores than Mi3, as expected, since it does not model pairwise epistasis by design. Its r_{20} scores are similar across all experiments, suggesting that it is not strongly affected by out-of-sample error. This is expected because its parameters are optimized for reproducing single-site frequency statistics only, which can be accurately estimated even from small training MSAs.⁴⁵ The r_{20} score for vVAE lies between Mi3 and Indep for all training datasets and n . With 1M training sequences, vVAE r_{20} decreases to 0.4 for $n = 10$, reflecting specification error (Fig. 2a). With 10K synthetic training sequences, vVAE r_{20} decreases further for all n due to the addition of out-of-sample error (Fig. 2e).

Whereas the pairwise covariation correlations represent a preliminary indication that vVAE captures epistasis but mispredicts its strength, the r_{20} results reinforce this finding and extend it into higher orders. Unlike Mi3, vVAE shows specification error even when fit to large datasets from a model which only contains pairwise epistatic interaction terms (Fig. 2d). Because higher-order covariation statistics are constrained by the pairwise statistics, and vVAE mispredicts the pairwise statistics, we expect that vVAE will exhibit specification error for higher-order epistasis, even though our synthetic test does not address this issue directly. When considered together with the r_{20} , the pairwise covariance correlations reveal a novel insight, which is that when trying to gauge GPSM generative capacity at higher orders of covariation, the pairwise statistics alone can be misleading. The relative magnitudes of r_{20} between models at $n = 2$ are different at higher n , and the performance decrease for high n is more severe for vVAE than Mi3 (Fig. 2, Bottom Row). We emphasize that the r_{20} performance decrease for Mi3 when tested against both synthetic and natural MSA targets can be accounted for entirely by out-of-sample error.

Hamming distance distributions

The next metric we use to characterize the generative capacity of the models is the pairwise Hamming distance distribution $d(S, S')$. The Hamming distance between two protein sequences is the number of amino acids that are different between them, and we obtain a distribution for an MSA by comparing all pairs of sequences. Because it characterizes the amount of sequence diversity in an MSA, recapitulation of the Hamming distance distribution has been used in the past as a measure for GPSM performance.^{2, 13, 36, 37} In Fig. 3, we compare the pairwise Hamming distance distribution for each GPSM to that of the target distribution, computed with evaluation and target MSAs of 10K sequences each. To quantify the difference between the GPSM and target distributions for this metric, we use the total variation distance (TVD),⁴⁶ which equals 1 when the distributions have no overlap and is 0 when they are identical, defined by $TVD[f, g] = 1/2 \int |f(x) - g(x)| dx$.

All models reproduce the mode Hamming distance of ~ 179 . For Mi3, we report $TVD = 0.007$ when trained on 1M (Fig. 3a) or 10K (Fig. 3b) synthetic sequences, showing no specification error, as expected. When trained on 10K natural sequences, Mi3 TVD increases to 0.012 (Fig. 3c), for reasons discussed further below. Indep significantly underestimates the probability of low and high Hamming distances, as observed at the distribution tails, with $TVD 0.24$ across all experiments. vVAE performs in between Mi3 and Indep, but much closer to Mi3 than Indep with respect to TVD . These performance differences across all GPSMs appear to indicate that out-of-sample error has a consistent and detectable, though negligible, effect on the fundamental sequence diversity of artificial GPSM-generated MSAs. That Mi3 and vVAE are highly performant and comparable to each other, but not Indep, corroborates our earlier finding that epistasis is relevant to accurate modelling of protein sequence diversity (Fig. 2). However, because Indep performs much closer to Mi3 and vVAE for this metric than on any other metric, and also because this metric cannot discriminate well between Mi3 and vVAE, it could mean that reproducing the Hamming distance distribution is a much easier, and perhaps separate, hurdle for GPSMs than is reproducing higher-order covariation.

To emphasize the decay of the tails, we rescale all the distributions by their maxima and re-center them around their modes to give them the same peak, and then plot them on a log-log scale (Fig. 3, Bottom Row). The relevance of the distribution's tails lies in their power-law behavior as they approach zero, where the function's exponent is related to the intrinsic dimension of the dataset and therefore to the number of informative latent factors needed to explain the data.^{36, 37, 47} A well specified generative model ought to reproduce this exponent, and therefore the tail's decay, since it is a topological property intrinsic to the dataset and independent from the particular choice of variables used to describe the probability density.⁴⁷ The trend of slightly decreasing generative capacity as training samples decrease, as observed in Fig. 3, Top Row, is emphasized in Fig. 3, Bottom Row. In this rendering of the Hamming distance distribution, differences in GPSM generative capacity can be observed at both low (Left Tail) and high (Right Tail) sequence diversity. The Mi3 distribution closely overlaps the target distribution with both 1M (Fig. 3d) and 10K (Fig. 3e) synthetic training sequences. In the 10K natural experiment, Mi3 deviates noticeably from the target on the left tail (Fig. 3f), which represents less evolutionarily diverged sequences. This could be an

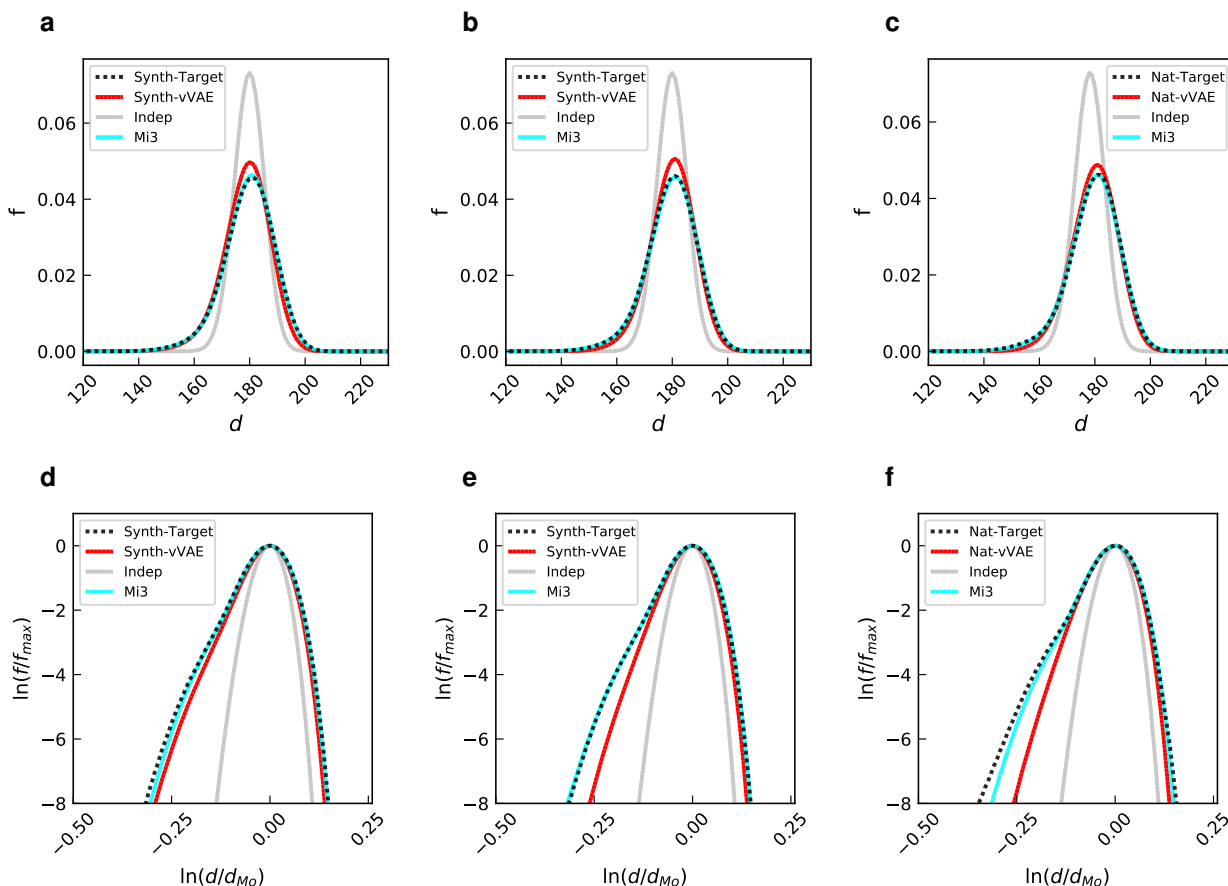


Figure 3. Pairwise Hamming distance distributions. These plots illustrate whether sequences generated from the GPSMs reproduce the overall sequence diversity of their respective targets. Mi3 (cyan), vVAE (red), and Indep (gray) distributions are compared to target distribution (dotted black). GPSMs were trained on 1M synthetic (a, d), 10K synthetic (b, e), or 10K natural (c, f) sequences from the corresponding target distribution. All Hamming distributions were computed from 30K-sequence evaluation MSAs, except for the natural target, which was computed from a 10K-sequence target MSA due to data limitations. **Top Row**, Hamming distances d (x-axis) are shown about the mode, and frequency f is normalized as a fraction of total (y-axis). Mi3 perfectly matches the target distribution, and vVAE performs closely to Mi3. **Bottom Row**, Re-scaled logarithmic Hamming distance distributions better discriminate between GPSMs with respect to generative capacity than the normal Hamming distance distribution. Before being log-scaled, the Hamming distances d are normalized by the mode d_{Mo} (x-axis), and frequencies f are normalized by the maximum Hamming distance f_{max} (y-axis). This transformation highlights minute differences between distributions at low frequencies in the tails of the distributions on the left- and right-hand sides. Only vVAE appears sensitive to training sample size for this metric at the log-log scale.

artifact of the phylogenetic relationships between sequences present in the natural dataset, which may have been incompletely removed by our phylogenetic filtering step for this data (see Methods, Supplement), or it could be due to estimation error in measuring the target distribution, as only 10K target sequences are available to estimate the black line in the natural analysis. As before, Indep performance is consistently low across all experiments. vVAE performance at low sequence diversity (Fig. 3, Bottom Row, Left Tails) decreases for smaller training dataset size.

Energy Correlations

A fourth metric we use to evaluate generative capacity is statistical energy $E(S)$ of individual sequences in the dataset, which we express using the negative logarithm of the predicted sequence probability $p(S)$, where $E(S) = -\log p(S)$. $E(S)$ can be computed analytically for Mi3 and Indep, and estimated for vVAE by importance sampling (see Methods).

This statistic directly evaluates accuracy of the GPSM distribution values $p_{\theta}(S)$ for a limited number of individual sequences, which has been used to validate GPSMs by comparison to corresponding experimental fitness values.^{13,19,48,49} In Fig. 4, we compare artificial statistical energies from the GPSM distribution $p_{\theta}(S)$ to those of the target distribution $p^0(S)$ for a 1K test MSA generated from $p^0(S)$. As before, we use the 1M (Fig. 4, Left Column) and 10K (Fig. 4, Right Column) training MSA sizes, and quantify GPSM generative capacity for this metric by the Pearson correlation coefficient $\rho(\{E(S)\}, \{\hat{E}(S)\})$ between GPSM and target energies. Mi3 reproduces the synthetic target distribution at both training MSA sizes. Because Mi3 should have very low specification error on the

synthetic target, as it is well specified by design, the small amount of error must be due to remaining out-of-sample or numerical errors. As expected, Indep relatively poorly reproduces the target values, with $\rho = 0.6$ for both MSA training sizes. vVAE exhibits greater specification error than Mi3 on the 1M training set with correlation of $\rho = 0.94$, and exhibits further out-of-sample error on the 10K training set with $\rho = 0.89$.

Conclusions

In this study we reveal for the first time the steep challenges, limits, and errors faced by contemporaneous GPSMs trained on either synthetic or currently available natural sequence datasets. Recent state-of-the-art GPSM studies have benchmarked the models by comparing $p_{\theta}(S)$ to experimental fitness values for single and double point mutations,^{19,21} or by generating artificial sequences that appear to fold into realistic structures based on *in silico* folding energy.²⁴ However, these strategies for model comparison present their own challenges. Point mutation fitness experiments in practice may measure particular contributors to fitness, including replicative capacity, drug resistance, protein stability, and enzymatic activity,¹⁹ and are subject to significant experimental error and other limitations, e.g. those imposed by conservation.⁵⁰ On the other hand, *in silico* computational chemistry approaches rely on energy functionals that may lack the precision needed to meaningfully discriminate between highly similar sequences.⁵¹ Additionally, neither protein function nor fitness rely exclusively on the thermodynamic stability of the static native structure, but more so on the protein's conformational dynamics,^{52–56} which are not fully described by folding energy values alone.⁵⁷ This could mean that despite generating sequences with realistic *in silico* folding energy, a GPSM may still not be capturing crucial higher-order epistasis effects. Neither point mutation fitness effects, nor *in silico* folding energy estimations, are directly related to mutational covariation statistics observed in an MSA, and thus they are indirect metrics of GPSM statistical accuracy. Comparing higher-order covariation patterns between target MSAs and GPSM-generated evaluation MSAs, as we do here, is a direct measurement of GPSM statistical accuracy, and our study emphasizes higher-order covariation whereas previous studies rarely go beyond the pairwise level.^{2,13,34,35,58}

Benchmarking coevolution-based protein sequence models in data rich and data poor regimes, as done here, is an effective method for ascertaining where data-driven effects stop, and algorithmic failure begins.³⁹ In our synthetic analysis track, we have demonstrated the extent to which a vanilla VAE (vVAE) can capture higher-order covariation at orders between three and ten when the target distribution is known, its statistical properties are measurable with a high degree of certainty, and major forms of error are removed, minimized, or accounted for. When given a large number of training and target sequences, we found vVAE's generative capacity to be between that of an site-independent model (Indep) and a pairwise Hamiltonian (Mi3) for all measurements. In the synthetic r_{20} experiments, our results show that vVAE generative capacity is well below Mi3, raising questions about whether vanilla VAEs can capture higher-order epistasis significantly better than a pairwise Potts model.

The Hamming distance distributions, pairwise covariation correlations, and energy correlations have been used in the past to measure GPSM accuracy, but we find that they can be inadequate or misleading indicators of a GPSM's ability to capture covariation at higher orders. Taken together, our results suggest that, of the metrics we tested, only r_{20} provides the granularity needed to discriminate between different GPSM's ability to model epistasis, because r_{20} most directly tests the model's ability to capture higher-order covariation.

Comparative benchmarking of our r_{20} results between the natural and synthetic analyses has shown for the first time how inherent limitations of natural sequence data preclude insights about GPSM performance, with respect to higher-order covariation. Our results also show that there are too few sequences in typical natural datasets to accurately gauge the generative capacity of a GPSM, without also performing a synthetic test. In our natural analysis, both the training and model evaluation processes are data-starved to the degree typical of publicly available protein sequence datasets, allowing out-of-sample and estimation error to frustrate efforts to discriminate between model performance.

Although our results suggest VAE-GPSMs are less effective for capturing higher-order epistasis, they have demonstrated utility in unsupervised learning and clustering. One VAE-GPSM has generated artificial sequences that share a "hallucinated" homology to natural proteins in the training set, which could mean that their folded structures would perform similar functions to their hallucinated natural homologs.²² Another has shown that a VAE-GPSM's latent space may capture phylogenetic relationships²⁰ better than PCA⁵⁹ and t-SNE.⁶⁰ These VAE-GPSMs furnished a latent space that immediately allowed for function-based protein classification, a benefit unavailable to pairwise Potts models without some effort.

Our suite of generative capacity metrics focus on higher-order covariation, with the potential for broad applicability to various sequentially ordered data. These measurements become possible when the data are sufficient in number, and the correlation structures between items, both within and across samples, are statistically detectable and

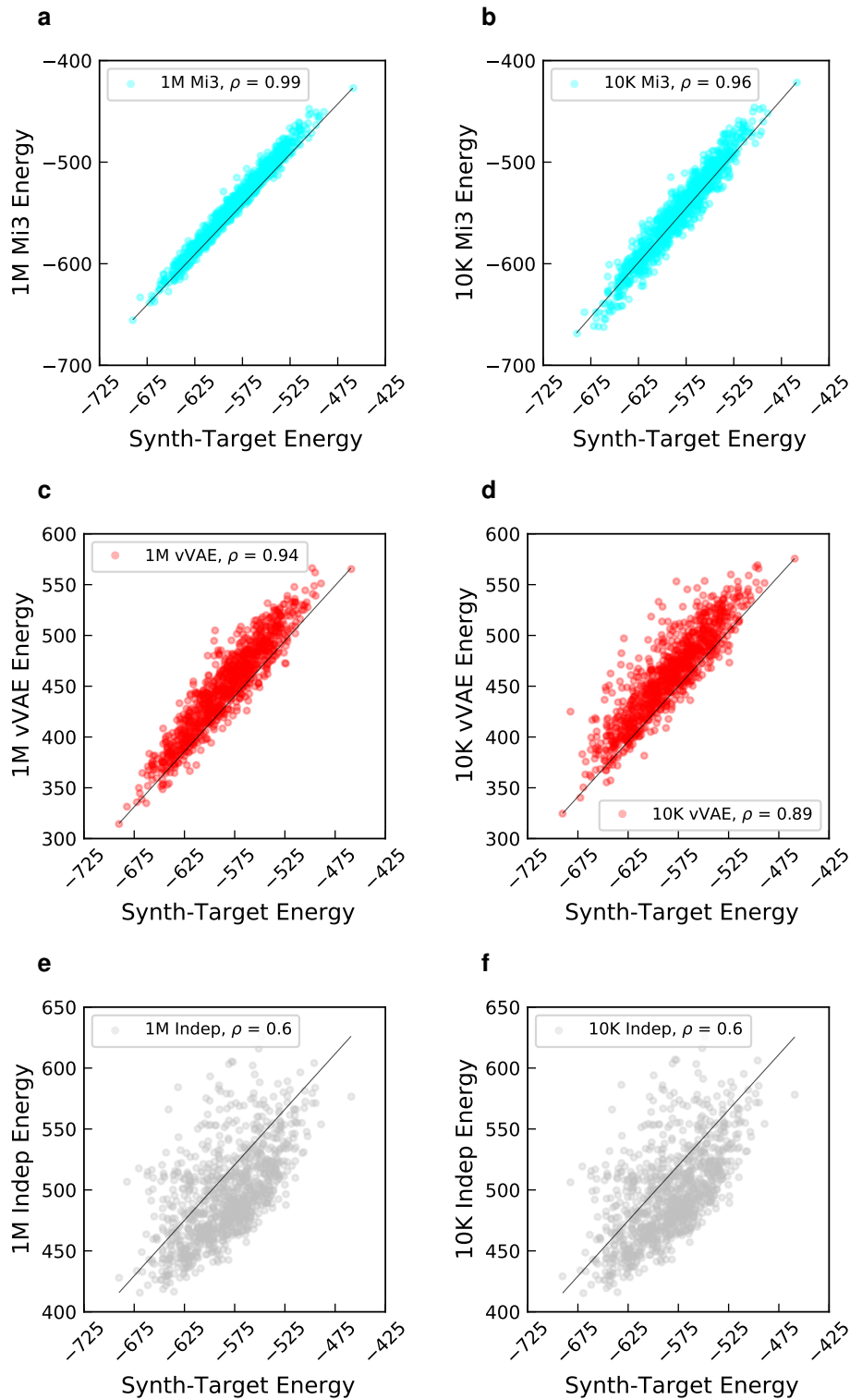


Figure 4. Statistical energy correlations. Statistical energies $E(S)$ of 1K synthetic test sequences from the target distribution as evaluated by Mi3 (cyan), vVAE (red), Indep (gray). Each GPSM was trained on 1M (a, c, e) or 10K (b, d, f) sequences from the synthetic target distribution. For each scatterplot, Pearson correlation coefficient ρ was computed between each GPSM’s statistical energy and that of the synthetic target distribution for each sequence. Only Indep is insensitive to decreased training sample size for this metric.

meaningful in some context, be it visual, biophysical, or linguistic. The convergence between images, proteins, and language with respect to generative modelling evaluation offers the exciting opportunity of a wider, interdisciplinary audience for the work proposed here. Most importantly, our metrics suite and overall approach represent not only a revision of currently prevailing paradigms of GPSM benchmarking, but also a challenge to generative modelling more broadly, to consider how higher-order covariation metrics and epistasis can inform their models and results.

Methods

Sequence dataset preparation

For the natural analysis, we use an MSA of the kinase protein superfamily which we have previously curated using sequences from the Uniprot/TREMBL database.⁴⁰ This MSA is composed of $\sim 20\text{K}$ sequences of length 232, obtained by filtering a larger set of $\sim 291\text{K}$ sequences to remove any sequences with more than 50% sequence identity to another (see Supplement).

For the synthetic analysis, synthetic sequences are generated from an “original” Potts Hamiltonian model trained on the natural protein-kinase MSA, as detailed below and shown in Fig. 1, Stage 1. This synthetic MSA is considered to be the target for the synthetic analysis. To clarify, our focus in this work is to quantify model generative capacity against the target distribution, and not the training distribution itself. Therefore, we have ensured that our synthetic training and target sequences are non-overlapping sets, even though they come from the same target model. The statistical differences between the two sets are nontrivial, and have been detected experimentally by our measurements (see Results).

In Stage 2, we process the sequences into a train-validation-test split. The processed MSAs are then one-hot encoded and fed into the GPSMs in Stage 3, where training occurs. In Stage 4, we generate artificial MSAs from each model, and in Stage 5 we perform our generative capacity measurements by comparing the artificial MSAs to the appropriate target MSA.

Mi3

The Mi3 model is a pairwise Potts Hamiltonian model fit to sequence data using the “Mi3-GPU” software we have developed previously,³² which performs “inverse Ising inference” to infer parameters of Potts models using a Markov-Chain Monte-Carlo (MCMC) algorithm which entails very few approximations. This software allows us to fit statistically accurate Potts models to MSA data. We have examined Mi3’s generative capacity and out-of-sample error in earlier work,^{32,45} which we summarize here.

A Potts model is the maximum entropy model for $p(S)$ constrained to reproduce the bivariate marginals $f_{\alpha\beta}^{ij}$ of an MSA, i.e. the frequency of amino acid combination α, β , at positions i, j . The probability distribution $p_{\theta}(S)$ for the Potts model takes the form

$$p_{\theta}(S) = \frac{e^{-E(S)}}{Z} \quad \text{with} \quad E(S) = \sum_i h_{s_i}^i + \sum_{i < j} J_{s_i s_j}^{ij} \quad (1)$$

where Z is a normalization constant, $Z = \sum_S e^{-E(S)}$, and “coupling” $J_{\alpha\beta}^{ij}$ and “field” h_{α}^i parameters are compactly denoted by the vector $\theta = \{h_{\alpha}^i, J_{\alpha\beta}^{ij}\}$. The number of free parameters of the model (non-independent couplings and fields) is equal to the number of non-independent bivariate marginals, which can be shown to be $\frac{L(L-1)}{2}(q-1)^2 + L(q-1)$ for q amino acids,¹⁵ which is 10.7M parameters for our model. This implies that the Potts model is well specified to reproduce the bivariate marginals when generating sequences from $p_{\theta}(S)$.

The Mi3 model inference procedure maximizes the log-likelihood with regularization. Maximizing the Potts log-likelihood can be shown to be equivalent to minimizing the difference between the dataset MSA bivariate marginals $f_{\alpha\beta}^{ij}$ and the model bivariate marginals of sequences generated from $p(S)$. To account for finite sampling error in the estimate of $f_{\alpha\beta}^{ij}$ for an MSA of N sequences we add a small pseudocount of size $1/N$, as described previously.⁴⁵ We also add a regularization penalty to the likelihood affecting the coupling parameters $J_{\alpha\beta}^{ij}$ to bias them towards 0, of form $\lambda \sum \text{SCAD}(J_{\alpha\beta}^{ij}, \lambda, \alpha)$ using the SCAD function which behaves like $\lambda |J_{\alpha\beta}^{ij}|$ for small $J_{\alpha\beta}^{ij}$ but gives no bias for large $J_{\alpha\beta}^{ij}$ ⁶¹, using a small regularization strength of $\lambda = 0.001$ for all inferences which causes little model bias.

To generate synthetic MSAs from the Potts model we use MCMC over the trial distribution $p_{\theta}(S)$ until the Markov-Chains reach equilibrium, as described previously.³² We can directly evaluate $E(S)$ the negative log-probability of

any sequences for the Mi3 model using equation 1 up to a constant Z , and this constant can be dropped without affecting our results.

Indep

The Indep model is the maximum entropy model for $p(S)$ constrained to reproduce the univariate marginals of an MSA, and is commonly called a “site-independent” model because the sequence variations at each site are independent of the variation at other sites. Because it does not fit the bivariate marginals, it cannot model covariation between positions. It takes the form

$$p_{\theta}(S) = \frac{e^{-E(S)}}{Z} \quad \text{with} \quad E(S) = \sum_i^L h_{s_i}^i \quad (2)$$

where Z is a normalization constant, $Z = \sum_S e^{-E(S)}$, and “field” parameters h_{α}^i for all positions i and amino acids α are compactly referred to by the vector $\theta = \{h_{\alpha}^i\}$. The fields of the Indep model generally have different values from the fields of the Potts model. Unlike for the Potts model, maximum likelihood parameters can be determined analytically to be $h_{\alpha}^i = -\log f_{\alpha}^i$ where f_{α}^i are the univariate marginals of the dataset MSA. When fitting the Indep model to a dataset MSA of N sequences, we add a pseudocount of $1/N$ to the univariate marginals to give model marginals \hat{f}_{α}^i , to account for finite sample error in the univariate marginal estimates. The model distribution simplifies to a product over positions, as $p_{\theta}(S) = \prod \hat{f}_{s_i}^i$. The number of independent field parameters is $L(q-1)$ which equals 4.6K parameters for our model.

To generate sequences from the independent model we independently generate the residues at each position i by a weighted random sample from the marginals \hat{f}_{α}^i , and we directly evaluate the log probability of each sequence $E(S)$ from equation 2.

vVAE

The vanilla variational autoencoder (vVAE) is a deep, symmetrical, and undercomplete autoencoder neural network composed of a separate encoder $q_{\phi}(Z|S)$ and decoder $p_{\theta}(S|Z)$,⁶² which map input sequences S to regions within a low-dimensional latent space Z and back. The probability distribution for the vVAE is defined as

$$p_{\theta}(S) = \int p_{\theta}(S|Z)p(Z)dZ \quad (3)$$

where the latent space distribution is a unit Normal distribution, $p(Z) = \mathcal{N}[0, 1](Z)$. Training of a VAE can be understood as maximization of the dataset log-likelihood with the addition of a Kullback-Leibler regularization term $D_{\text{KL}}[q_{\phi}(Z|S), p_{\theta}(Z|S)]$, where $p_{\theta}(Z|S)$ is the posterior of the decoder.^{28,29}

Our VAE architecture is intentionally “vanilla”,³³ and our encoder and decoder use a simple architecture unlike more sophisticated VAE implementations which use convolutional layers,¹⁹ multi-stage training,⁶³ disentanglement learning,³³ Riemannian Brownian motion priors,⁶⁴ and more. It reflects a simple VAE architecture that has been implemented as a VAE-GPSM in prior work.²¹ This allows us to directly interrogate the assumptions and performance of vanilla variational autoencoding with respect to the training and evaluation of GPSMs in this work.

Our encoder and decoder have 3 layers each and employ minimal standard normalization and regularization strategies. vVAE’s latent bottleneck layer has 7 nodes, and the model in total has 2.7M inferred parameters. The input layer of the encoder accepts a one-hot encoded sequence and the decoder’s output layer values can be interpreted as a Bernoulli distribution of the same dimensions as a one-hot encoded sequence. We have tested various vanilla VAE architectures and hyperparameters with our datasets, as well as DeepSequence,¹⁹ and found qualitatively similar generative capacity results.

To generate a sequence from vVAE, we generate a random sample in latent space from the latent distribution $p(Z)$ pass this value to the decoder to obtain a Bernoulli distribution, from which we sample once. To evaluate the negative log-probability of a sequence $E(S)$ we use importance sampling, averaging over 1K samples from the latent distribution $q_{\phi}(Z|S)$.²⁰ Other publications use the Evidence Lower Bound (ELBO) estimate as an approximation of the negative log-probability,¹⁹ and we have verified that the ELBO and the negative log-probability are nearly identical in our tests and have equal computational complexity.

References

1. Levy, R. M., Haldane, A. & Flynn, W. F. Potts hamiltonian models of protein co-variation, free energy landscapes, and evolutionary fitness. *Current Opinion in Structural Biology* **43**, 55–62 (2017).

2. Cocco, S., Feinauer, C., Figliuzzi, M., Monasson, R. & Weigt, M. Inverse statistical physics of protein sequences: a key issues review. *Reports on Progress in Physics* **81**, 032601 (2018). Publisher: IOP Publishing.
3. Tubiana, J., Cocco, S. & Monasson, R. Learning compositional representations of interacting systems with restricted boltzmann machines: Comparative study of lattice proteins. *Neural Computation* **31**, 1671–1717 (2019). URL https://doi.org/10.1162/neco_a_01210.
4. Lapedes, A. S., Giraud, B., Liu, L. & Stormo, G. D. *Correlated mutations in models of protein sequences: phylogenetic and structural effects* (Institute of Mathematical Statistics, 1999). Pages: 236-256 Publication Title: Statistics in molecular biology and genetics.
5. Weigt, M., White, R. A., Szurmant, H., Hoch, J. A. & Hwa, T. Identification of direct residue contacts in protein–protein interaction by message passing. *Proceedings of the National Academy of Sciences* **106**, 67–72 (2009). Publisher: National Academy of Sciences Section: Physical Sciences.
6. Haldane, A., Flynn, W. F., He, P., Vijayan, R. S. K. & Levy, R. M. Structural propensities of kinase family proteins from a Potts model of residue co-variation. *Protein Science: A Publication of the Protein Society* **25**, 1378–1384 (2016).
7. Domingo, J., Baeza-Centurion, P. & Lehner, B. The Causes and Consequences of Genetic Interactions (Epistasis). *Annual Review of Genomics and Human Genetics* **20**, 433–460 (2019). Publisher: Annual Reviews.
8. Noel, J. K., Morcos, F. & Onuchic, J. N. Sequence co-evolutionary information is a natural partner to minimally-frustrated models of biomolecular dynamics. *F1000Research* **5** (2016). URL <https://www.ncbi.nlm.nih.gov/pmc/articles/PMC4755392/>.
9. Morcos, F., Jana, B., Hwa, T. & Onuchic, J. N. Coevolutionary signals across protein lineages help capture multiple protein conformations. *Proceedings of the National Academy of Sciences* **110**, 20533–20538 (2013). URL <https://www.pnas.org/content/110/51/20533>. Publisher: National Academy of Sciences Section: Biological Sciences.
10. Sułkowska, J. I., Morcos, F., Weigt, M., Hwa, T. & Onuchic, J. N. Genomics-aided structure prediction. *Proceedings of the National Academy of Sciences* **109**, 10340–10345 (2012). URL <https://www.pnas.org/content/109/26/10340>. Publisher: National Academy of Sciences Section: Biological Sciences.
11. Hopf, T. A. *et al.* Mutation effects predicted from sequence co-variation. *Nature biotechnology* **35**, 128–135 (2017).
12. Biswas, A., Haldane, A., Arnold, E. & Levy, R. M. Epistasis and entrenchment of drug resistance in HIV-1 subtype B. *eLife* **8**, e50524 (2019). Publisher: eLife Sciences Publications, Ltd.
13. Haldane, A., Flynn, W. F., He, P. & Levy, R. M. Coevolutionary Landscape of Kinase Family Proteins: Sequence Probabilities and Functional Motifs. *Biophysical Journal* **114**, 21–31 (2018).
14. Figliuzzi, M., Barrat-Charlaix, P. & Weigt, M. How Pairwise Coevolutionary Models Capture the Collective Residue Variability in Proteins? *Molecular Biology and Evolution* **35**, 1018–1027 (2018). URL <https://doi.org/10.1093/molbev/msy007>. <https://academic.oup.com/mbe/article-pdf/35/4/1018/24597926/msy007.pdf>.
15. Bialek, W. & Ranganathan, R. Rediscovering the power of pairwise interactions. *arXiv:0712.4397 [q-bio]* (2007). ArXiv: 0712.4397.
16. Weinreich, D. M., Lan, Y., Wylie, C. S. & Heckendorn, R. B. Should evolutionary geneticists worry about higher-order epistasis? *Current opinion in genetics & development* **23**, 700–707 (2013).
17. Haq, O., Andrec, M., Morozov, A. V. & Levy, R. M. Correlated electrostatic mutations provide a reservoir of stability in hiv protease. *PLoS Comput Biol* **8**, e1002675EP (2012).
18. Haq, O., Levy, R., Morozov, A. & Andrec, M. Pairwise and higher-order correlations among drug-resistance mutations in hiv-1 subtype b protease. *BMC Bioinformatics* **10**, S10 (2009).
19. Riesselman, A. J., Ingraham, J. B. & Marks, D. S. Deep generative models of genetic variation capture the effects of mutations. *Nature Methods* **15**, 816–822 (2018).
20. Ding, X., Zou, Z. & Brooks lii, C. L. Deciphering protein evolution and fitness landscapes with latent space models. *Nature Communications* **10**, 5644 (2019). Number: 1 Publisher: Nature Publishing Group.
21. Sinai, S., Kelsic, E., Church, G. M. & Nowak, M. A. Variational auto-encoding of protein sequences. *arXiv:1712.03346 [cs, q-bio]* (2018). ArXiv: 1712.03346.

22. Costello, Z. & Martin, H. G. How to Hallucinate Functional Proteins. *arXiv:1903.00458 [q-bio]* (2019). ArXiv: 1903.00458.
23. Gupta, A. & Zou, J. Feedback GAN for DNA optimizes protein functions. *Nature Machine Intelligence* **1**, 105–111 (2019). Number: 2 Publisher: Nature Publishing Group.
24. Madani, A. *et al.* ProGen: Language Modeling for Protein Generation. *arXiv:2004.03497 [cs, q-bio, stat]* (2020). ArXiv: 2004.03497.
25. Vig, J. *et al.* BERTology Meets Biology: Interpreting Attention in Protein Language Models. *bioRxiv* 2020.06.26.174417 (2020). Publisher: Cold Spring Harbor Laboratory Section: New Results.
26. Elnaggar, A. *et al.* ProtTrans: Towards Cracking the Language of Life's Code Through Self-Supervised Deep Learning and High Performance Computing. *bioRxiv* 2020.07.12.199554 (2020). Publisher: Cold Spring Harbor Laboratory Section: New Results.
27. Choromanski, K. *et al.* Rethinking attention with performers. *CoRR abs/2009.14794* (2020). URL <https://arxiv.org/abs/2009.14794>. 2009.14794.
28. Kingma, D. P. & Welling, M. Auto-Encoding Variational Bayes. *arXiv:1312.6114 [cs, stat]* (2014). URL <http://arxiv.org/abs/1312.6114>. ArXiv: 1312.6114.
29. Rezende, D. J., Mohamed, S. & Wierstra, D. Stochastic Backpropagation and Approximate Inference in Deep Generative Models. *arXiv:1401.4082 [cs, stat]* (2014). ArXiv: 1401.4082.
30. Luce, R. D., Bush, R. R. & Galanter, E. (eds.) *Handbook of mathematical psychology: I.* Handbook of mathematical psychology: I. (John Wiley, Oxford, England, 1963). Pages: xiii, 491.
31. Frawley, W. J. *International Encyclopedia of Linguistics* (Oxford University Press, 2003). Publication Title: International Encyclopedia of Linguistics.
32. Haldane, A. & Levy, R. M. Mi3-GPU: MCMC-based inverse Ising inference on GPUs for protein covariation analysis. *Computer Physics Communications* 107312 (2020).
33. Ding, Z. *et al.* Guided Variational Autoencoder for Disentanglement Learning. *arXiv:2004.01255 [cs]* (2020). ArXiv: 2004.01255.
34. Shimagaki, K. & Weigt, M. Selection of sequence motifs and generative Hopfield-Potts models for protein families. *Physical Review E* **100**, 032128 (2019). URL <https://link.aps.org/doi/10.1103/PhysRevE.100.032128>. Publisher: American Physical Society.
35. Hawkins-Hooker, A. *et al.* Generating functional protein variants with variational autoencoders. *bioRxiv* 2020.04.07.029264 (2020). Publisher: Cold Spring Harbor Laboratory Section: New Results.
36. Facco, E., Pagnani, A., Russo, E. T. & Laio, A. The intrinsic dimension of protein sequence evolution. *PLOS Computational Biology* **15**, e1006767 (2019). Publisher: Public Library of Science.
37. Granata, D. & Carnevale, V. Accurate Estimation of the Intrinsic Dimension Using Graph Distances: Unraveling the Geometric Complexity of Datasets. *Scientific Reports* **6**, 31377 (2016).
38. El-Gebali, S. *et al.* The Pfam protein families database in 2019. *Nucleic Acids Research* **47**, D427–D432 (2019). Publisher: Oxford Academic.
39. AlQuraishi, M. ProteinNet: a standardized data set for machine learning of protein structure. *BMC Bioinformatics* **20**, 311 (2019). URL <https://doi.org/10.1186/s12859-019-2932-0>.
40. Consortium, T. U. UniProt: a worldwide hub of protein knowledge. *Nucleic Acids Research* **47**, D506–D515 (2019). URL <https://academic.oup.com/nar/article/47/D1/D506/5160987>. Publisher: Oxford Academic.
41. Burnham, K. P. & Anderson, D. R. *Model Selection and Multimodel Inference: A Practical Information-Theoretic Approach* (Springer-Verlag, New York, 2002), 2 edn.
42. Yaser S. Abu-Mostafa, Malik Magdon-Ismael, Hsuan-Tien Lin-Learning From Data_ A short course-AMLBook.com (2012).pdf | Statistical Classification | Machine Learning.
43. Everitt, B. S. & Skrondal, A. The Cambridge Dictionary of Statistics. *Cambridge University Press* 480 (2010).
44. Mohri, M., Rostamizadeh, A. & Talwalkar, A. *Foundations of Machine Learning, second edition* (MIT Press, 2018). Google-Books-ID: dWB9DwAAQBAJ.

45. Haldane, A. & Levy, R. M. Influence of multiple-sequence-alignment depth on Potts statistical models of protein covariation. *Physical Review. E* **99**, 032405 (2019).
46. Levin, D. A. & Peres, Y. *Markov Chains and Mixing Times* (American Mathematical Soc., 2017). Google-Books-ID: f208DwAAQBAJ.
47. Ansuini, A., Laio, A., Macke, J. H. & Zoccolan, D. Intrinsic dimension of data representations in deep neural networks. In *Advances in Neural Information Processing Systems*, 6111–6122 (2019).
48. Riesselman, A. *et al.* Accelerating Protein Design Using Autoregressive Generative Models. *bioRxiv* 757252 (2019). Publisher: Cold Spring Harbor Laboratory Section: New Results.
49. Figliuzzi, M., Jacquier, H., Schug, A., Tenaillon, O. & Weigt, M. Coevolutionary Landscape Inference and the Context-Dependence of Mutations in Beta-Lactamase TEM-1. *Molecular Biology and Evolution* **33**, 268–280 (2016).
50. Haddox, H. K., Dingens, A. S., Hilton, S. K., Overbaugh, J. & Bloom, J. D. Mapping mutational effects along the evolutionary landscape of HIV envelope. *eLife* **7**, e34420 (2018). Publisher: eLife Sciences Publications, Ltd.
51. Alley, E. C., Khimulya, G., Biswas, S., AlQuraishi, M. & Church, G. M. Unified rational protein engineering with sequence-based deep representation learning. *Nature Methods* **16**, 1315–1322 (2019). URL <https://www.nature.com/articles/s41592-019-0598-1>. Number: 12 Publisher: Nature Publishing Group.
52. Wei, G., Xi, W., Nussinov, R. & Ma, B. Protein Ensembles: How Does Nature Harness Thermodynamic Fluctuations for Life? The Diverse Functional Roles of Conformational Ensembles in the Cell. *Chemical Reviews* **116**, 6516–6551 (2016). URL <https://doi.org/10.1021/acs.chemrev.5b00562>. Publisher: American Chemical Society.
53. Anishchenko, I., Ovchinnikov, S., Kamisetty, H. & Baker, D. Origins of coevolution between residues distant in protein 3D structures. *Proceedings of the National Academy of Sciences* **114**, 9122–9127 (2017). URL <https://www.pnas.org/content/114/34/9122>. Publisher: National Academy of Sciences Section: Biological Sciences.
54. Sailer, Z. R. & Harms, M. J. Molecular ensembles make evolution unpredictable. *Proceedings of the National Academy of Sciences* **114**, 11938–11943 (2017). URL <https://www.pnas.org/content/114/45/11938>. Publisher: National Academy of Sciences Section: Biological Sciences.
55. Petrović, D., Risso, V. A., Kamerlin, S. C. L. & Sanchez-Ruiz, J. M. Conformational dynamics and enzyme evolution. *Journal of The Royal Society Interface* **15**, 20180330 (2018). URL <https://royalsocietypublishing.org/doi/full/10.1098/rsif.2018.0330>. Publisher: Royal Society.
56. Nussinov, R., Tsai, C.-J. & Jang, H. Protein ensembles link genotype to phenotype. *PLOS Computational Biology* **15**, e1006648 (2019). URL <https://journals.plos.org/ploscompbiol/article?id=10.1371/journal.pcbi.1006648>. Publisher: Public Library of Science.
57. Campitelli, P., Modi, T., Kumar, S. & Ozkan, S. B. The Role of Conformational Dynamics and Allostery in Modulating Protein Evolution. *Annual Review of Biophysics* **49**, 267–288 (2020). Publisher: Annual Reviews.
58. Haq, O., Levy, R. M., Morozov, A. V. & Andrec, M. Pairwise and higher-order correlations among drug-resistance mutations in HIV-1 subtype B protease. *BMC Bioinformatics* **10**, S10 (2009).
59. Bishop, C. M. *Pattern recognition and machine learning* (2006). ISBN: 9781493938438 9780387310732 Library Catalog: cds.cern.ch Publisher: Springer.
60. Maaten, L. v. d. & Hinton, G. Visualizing Data using t-SNE. *Journal of Machine Learning Research* **9**, 2579–2605 (2008).
61. Fan, J. & Li, R. Variable selection via nonconcave penalized likelihood and its oracle properties. *Journal of the American Statistical Association* **96**, 1348–1360 (2001). URL <https://doi.org/10.1198/016214501753382273>. <https://doi.org/10.1198/016214501753382273>.
62. Charte, D., Charte, F., García, S., del Jesus, M. J. & Herrera, F. A practical tutorial on autoencoders for nonlinear feature fusion: Taxonomy, models, software and guidelines. *Information Fusion* **44**, 78–96 (2018).
63. Dai, B. & Wipf, D. Diagnosing and Enhancing VAE Models. *arXiv:1903.05789 [cs, stat]* (2019). URL <http://arxiv.org/abs/1903.05789>. ArXiv: 1903.05789.
64. Kalatzis, D., Eklund, D., Arvanitidis, G. & Hauberg, S. Variational Autoencoders with Riemannian Brownian Motion Priors. *arXiv:2002.05227 [cs, stat]* (2020). ArXiv: 2002.05227.

Acknowledgements

This research was supported by the National Science Foundation, grant number NSF-GCR 1934848, and the National Institute of Health, grant number R35-GM132090. This research includes calculations carried out on HPC resources supported in part by the National Science Foundation through major research instrumentation grant number 1625061 and by the US Army Research Laboratory under contract number W911NF-16-2-0189.

Author contributions statement

F.M., R.M.L, V.C., A.H. conceived the experiments. F.M., V.C., A.H. performed the experiments. F.M., R.M.L, V.C., A.H. analyzed the results. F.M., V.C., A.H. wrote the bulk of the codebase, Q.N. made a contribution to the codebase. F.M., R.M.L, V.C., A.H. wrote the paper. All authors reviewed the manuscript.

Supplementary Information for: Generative Capacity of Probabilistic Protein Sequence Models

Francisco McGee Quentin Novinger Ronald M. Levy Vincenzo Carnevale Allan Haldane

1 vVAE implementation

The vanilla variational autoencoder (vVAE) is a deep, symmetrical, and undercomplete autoencoder neural network composed of a separate encoder $q_\phi(Z|S)$ and decoder $p_\theta(S|Z)$, which map input sequences S to regions of a low-dimensional latent space Z and back¹. It is a probabilistic model, and in our implementation we assume sequences will be distributed according to a unit normal distribution in latent space, $p(Z) = \mathcal{N}[0, 1](Z)$, as demonstrated in Ref.¹. Training of a VAE can be understood as maximization of (the logarithm of) the dataset likelihood $\mathcal{L} = \sum_S p_\theta(S) = \sum_S \int p_\theta(S|Z)p(Z)dZ$ with the addition of a Kullback-Leibler regularization term $D_{\text{KL}}[q_\phi(Z|S), p_\theta(Z|S)]$, where $p_\theta(Z|S)$ is the posterior of the decoder, which allows use of the fitted encoder $q_\phi(Z|S)$ to perform efficient estimation of the likelihood and its gradient by Monte-Carlo sampling, for appropriate encoder models.

Our vVAE architecture is built on the same basic VAE architecture described in Ref.², which itself appears to be built on the VAE implementation provided with the Keras library³. It is composed of 3 symmetrical ELU-activated layers in both the encoder and decoder, each layer with 250 dense (fully-connected) nodes. The encoder and decoder are connected by a latent layer of l nodes, we use $l = 7$ in the main text. Our vVAE's input layer accepts one-hot encoded sequences, and the output layer is sigmoid-activated and its node values can be interpreted as a Bernoulli distribution of the same dimensions as a one-hot encoded sequence. The first layer of the encoder and the middle layer of the decoder have dropout regularization applied with 30% dropout rate, and the middle layer of the encoder uses Batch normalization with a batch size of 200. In all inferences, we hold out 10% of the training sequences as a validation dataset, and perform maximum likelihood optimization using the Keras "adam" stochastic gradient optimizer on the remaining 90%. After each training epoch we evaluate the loss function for the training and validation data subsets separately. We have tested using early-stopping regularization to stop inference once the validation loss has not decreased for three epochs in a row as in previous implementations, but this led to some variability in the model depending on when the early stopping criterion was reached. To avoid this variability in order to make different models more directly comparable, we instead fix the number of epochs to 32 for all models, since in the early stopping tests this led to near minimum training loss and validation loss, and did not lead to significant overfitting as would be apparent from an increase in the validation loss.

Our model was implemented using Keras building on the previous implementations of Refs.^{2,3}, however with a modification of the loss function relative to both of these, to remove a scaling factor of Lq on the reconstruction loss which may be used to avoid issues with local minima described further below. This prefactor leads to a non-unit variance of the latent space distribution of the dataset sequences, violating our definition that the latent space distribution should be Normal with unit variance, $p(Z) = \mathcal{N}[0, 1](Z)$. In the next section we show that after removing the prefactor the latent space distribution is approximately a unit Normal, which more closely follows the original VAE theory developed in Ref.¹. Our implementation is available at https://github.com/ahaldane/MSA_VAE.

To generate a sequence from the model we generate a random sample in latent space from the latent distribution $\mathcal{N}[0, 1]$, pass this value to the decoder to obtain a Bernoulli distribution, from which we sample once. To evaluate the log-probability of a sequence, we use importance sampling, averaging over 1000 samples from the latent distribution $q_\phi(Z|S)$ following from the relations^{4,5}

$$\begin{aligned} p_\theta(S) &= \int p_\theta(S|Z)p(Z)dZ = \int q_\phi(Z|S) \frac{p_\theta(S|Z)p(Z)}{q_\phi(Z|S)} dZ \\ &= \mathbb{E}_{Z \sim q_\phi(Z|S)} \left[\frac{p_\theta(S|Z)p(Z)}{q_\phi(Z|S)} \right] \approx \frac{1}{N} \sum_i^N \frac{p_\theta(S|Z^i)p(Z^i)}{q_\phi(Z^i|S)} \end{aligned} \quad (1)$$

where, Z^i are independent samples from $q_\phi(Z|S)$ and N a large number of samples. Here $q_\phi(Z|S)$ plays the role of a sampling bias function, biasing samples to regions of latent space which are likely to have generated the sequence, leading to an accurate Monte-Carlo estimate of $p_\theta(S)$. The value $p_\theta(S)$ can be converted to a unit-less statistical energy as $E(S) = -\log p_\theta(S)$ for direct comparison with Mi3 and Indep statistical energies.

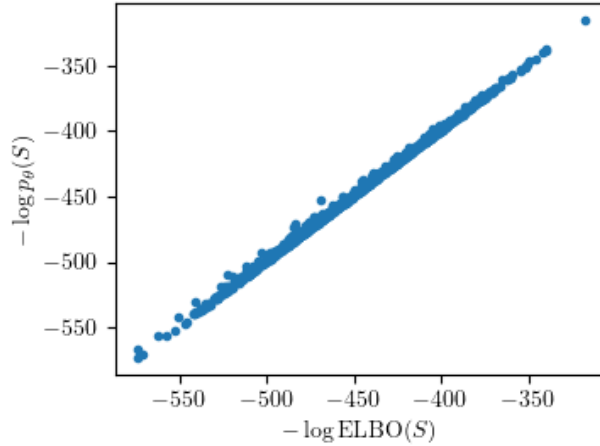


Figure 1. Comparison of $E(S) = -\log p_\theta(S)$ with the ELBO estimate for the vVAE with $l = 7$ fit to 1M sequences, evaluated for 1000 sequences S from the validation dataset, with $N = 1000$ samples for both the ELBO estimate and the $E(S)$ estimate.

Other publications have used the Evidence Lower Bound (ELBO) estimate as an approximation of $\log p_\theta(S)$ ⁶, and we have tested (see Fig. 1) that the ELBO and the log-probability are nearly identical, and $N = 1000$ samples is sufficient for an accurate estimate. The fact that the ELBO and log-probability are nearly identical is a sign that our encoder is well-fit, as the difference between these values should equal the KL divergence $D_{\text{KL}}[q_\phi(Z|S), p_\theta(Z|S)]$ between the “true” posterior of the decoder $p_\theta(Z|S)$ and the approximate posterior $q_\phi(Z|S)$, which should be 0 if the encoder $q_\phi(Z|S)$ has accurately modelled the posterior¹.

2 VAE model validation and generality

To validate our choice of latent space size of $l = 7$ used in the main text, we tried fitting vVAEs with different latent space sizes from 2 to 10. In Fig. 2 we illustrate the latent space projections of the sequences in the training dataset. According to our specification underlying the VAE theoretically, we expect the latent space distribution to be a multidimensional normal distribution with mean 0 and unit variance. Indeed, as can be seen in the plot (and measured numerically) generally we find latent space distribution of the dataset to have close to unit variance and is approximately Normal, although there is some non-Normal structure in the distribution.

For latent spaces of $l = 8$ and $l = 10$ we observe that some latent dimensions appear to have “collapsed”, in particular z_0 for $l = 8$, and z_1 and z_6 for $l = 10$. From repeated runs (not shown) we observe that the number of collapsed dimensions varies somewhat depending on the random seed used to initialize the stochastic optimizer, and also depends on the size of the training dataset as more dimensions collapse when fitting 1M sequences than fitting 10K sequences (not shown). For these “collapsed” dimensions, we see that the projected variance of the illustrated sequence in red in Fig. 2 is very close to 1.0, unlike in other dimensions where the projected variance is much smaller. These behaviors are consistent with a well known phenomenon of “posterior collapse” discussed in VAE literature⁷. It has been suggested that VAE posterior collapse can occur due to local minima in the likelihood function which are not global minima⁷, but in some situations can be a sign that additional latent dimensions are uninformative and fewer latent dimensions are needed to represent the data⁸. We find that choosing $l = 7$ gives the best performing model which avoids posterior collapse. Interestingly, the number of “informative” latent variables, *i.e.* those that do not undergo posterior collapse, turns out to coincide with the intrinsic dimension of the dataset of training sequences, estimated from the set of pairwise distances using a completely independent approach⁹. In brief, it has been shown⁹ that graph distances calculated on k-neighbor graphs can be used to approximate geodesics and thus to generate the distribution of “intrinsic” distances. Close to the maximum, the latter depends exclusively on the dimension of the distance distribution’s support. This observation is used to devise a family of estimators for the intrinsic dimension. Using these tools, we estimated an ID of 7 or 8 for the synthetic dataset used in the main text. Interestingly, these numbers are consistent with what observed in terms of collapse of the posterior distribution: the ID is seemingly related to the number of informative latent variables so that if the number of nodes in the embedding layer is increased past this number, posterior collapse occurs indicating that the additional variables are not needed to explain the data.

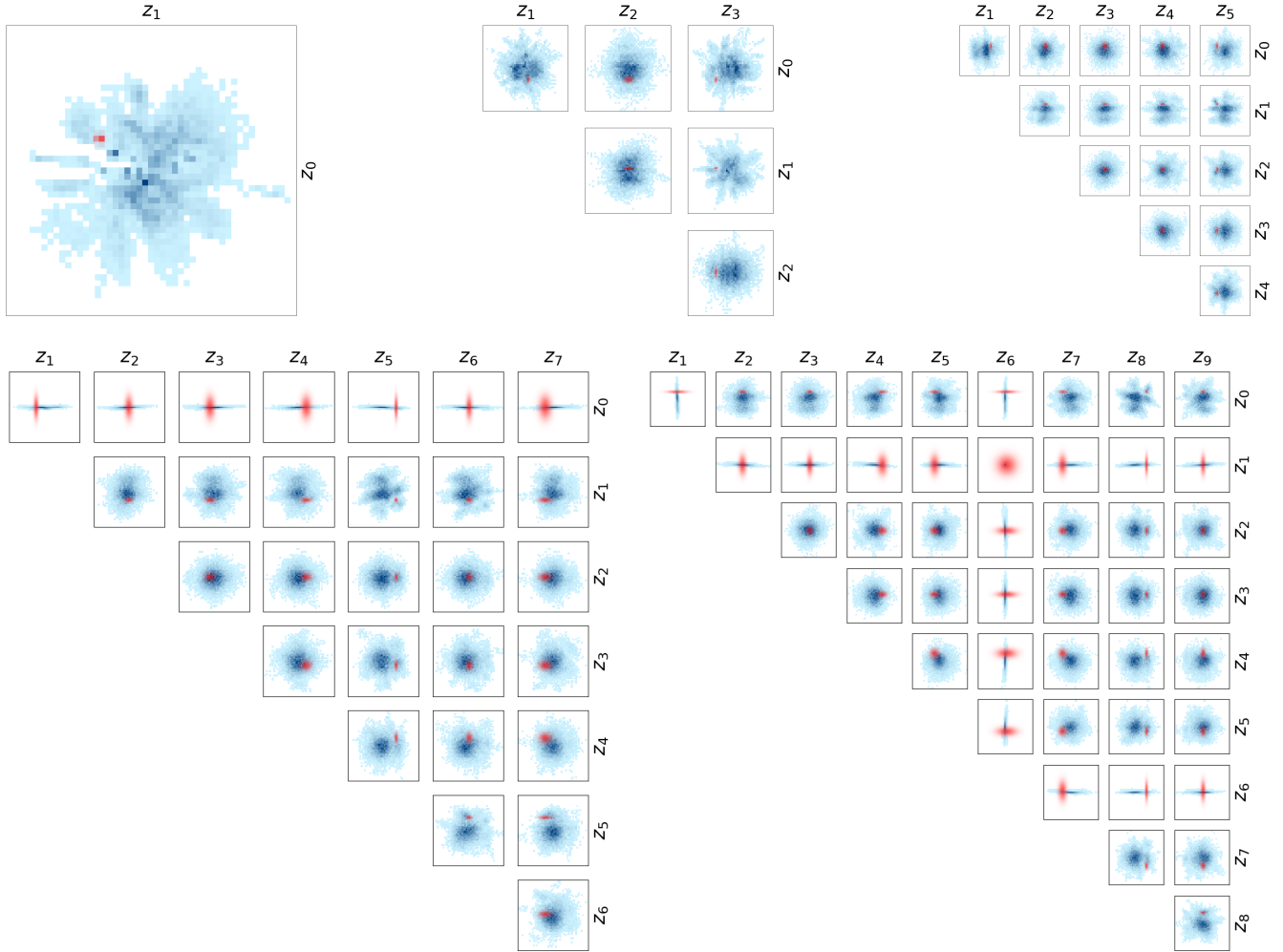


Figure 2. Plots of latent space distribution of the training dataset for vVAE models fit with different latent space sizes of 2, 4, 6, 8, and 10 (ordered from top left), fit to 1M synthetic training sequences as in the synthetic test in the main text. For each latent space size we show, for each pair of latent variables, a 2d histogram of the projected means of 10K training dataset sequences in latent space in blue. There is one subplot for $l=2$, six subplots for $l=4$, etc. Each plot ranges from -4 to 4 on both axes. The latent distribution $q_\phi(Z|S)$ for single random sequence from the training dataset is shown as a red shading in proportion to probability.

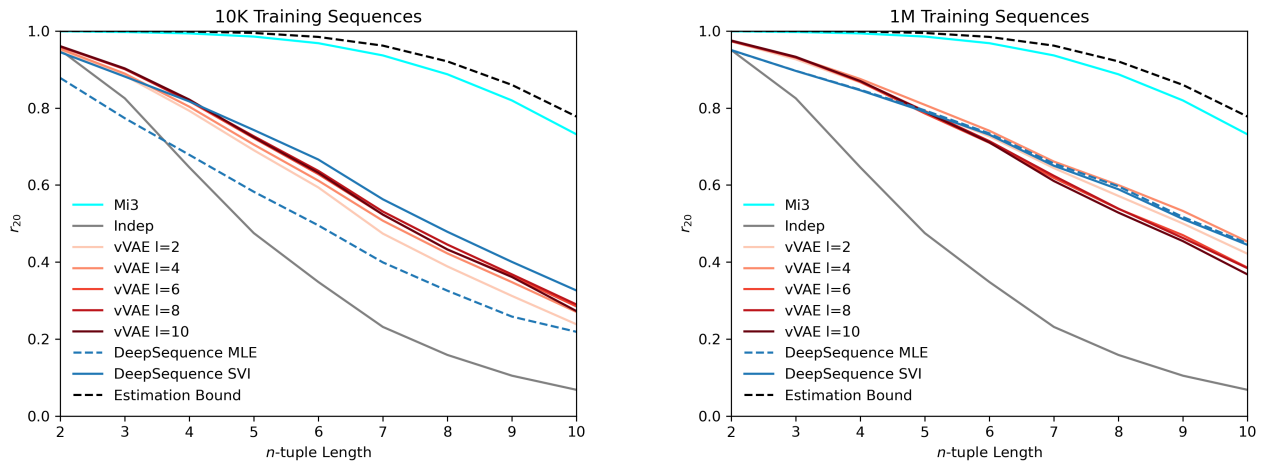


Figure 3. Performance comparison of vVAEs for different l and compared to DeepSequence VAEs and Mi3 using the r_{20} metric.

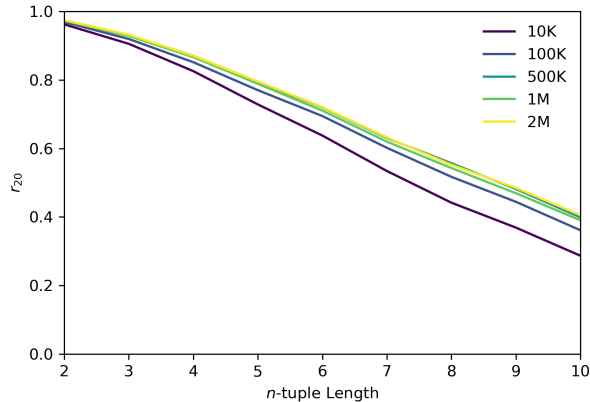


Figure 4. VVAE performance for $l = 7$ for varying training dataset sizes. For each training dataset size, two inferences are run with different random seeds, shown in solid and dashed lines for each training size.

To compare the generative capacity of different GPSMs to determine how general our results are, we computed our MSA statistics for other VAEs besides the $l = 7$ vVAE shown in the main text. In Fig. 3 we show the r_{20} scores for different models when fit to either 10K or 1M synthetic sequences, as in the synthetic tests in the main text. We include the Mi3 and Indep models, as well as vVAEs for different latent space sizes, and also models produced using the DeepSequence VAE software which comes in two variations, the "MLE" and the "SVI" algorithms⁶, for which we use the default or example parameters. All the VAEs perform fairly similarly in this metric, including the DeepSequence VAEs. For the smaller training dataset of 10K sequence the DeepSequence SVI algorithm outperforms the other VAEs, suggesting it is less susceptible to out-of-sample error. These results suggest that our results for the vVAE shown in the main text generalize to other VAEs, including the significantly more complex DeepSequence VAEs, and are not strongly dependent on implementation or number of latent variables l . The models with $l \sim 7$ perform among the best of the vVAE models for both the 10K and the 1M training datasets, though the difference between the models is small, and this further justifies our choice of $l = 7$ in the main text.

3 Minimizing VAE out-of-sample error

The goal of the synthetic test with 1M training sequences in the main text is to eliminate out-of-sample error (overfitting) by using an extremely large training dataset. How large must the training dataset be to mostly eliminate out-of-sample error for the vVAE? In Fig. 4 we show tests for the $l = 7$ vVAE for increasing training dataset sizes, finding that after 500K sequences the improvement in performance becomes small. This justifies our choice of using 1M synthetic sequences as there is little additional improvement to be gained by fitting to 2M sequences at the cost of increasingly prohibitive fitting time.

4 How higher-order Covariation is represented by Pairwise models

One of the questions we address in the main text is whether different GPSMs are well-specified to describe protein sequence variation, especially in the case of covariation of many positions in the sequence at once. Of particular interest is whether a model which explicitly includes only pairwise interactions such as the Potts model is sufficient to model higher order epistasis or whether GPSMs with more complex functional forms, such as the vVAE, are necessary.

Here for clarity we give a brief example describing how Potts models can predict many patterns of higher-order covariation, meaning triplet and higher patterns of residue covariation, despite only modelling pairwise interactions. We illustrate this using model describing sequences of length $L = 3$ with two residue types A and B, with $2^3 = 8$ possible sequences, and show different forms of higher-order covariation which a pairwise model can and cannot fit. We refer to Refs¹⁰⁻¹² for detailed discussion of these issues and theoretical results suggesting why pairwise models are often sufficient to model many datasets.

First, we show how such a Potts model generates triplet covariation. Consider a Potts model with parameters given by $J_{AA}^{12} = J_{AA}^{23} = -s$ for some interaction strength s and all other field and coupling parameters are 0. This directly couples the character "A" between positions (1,2) and also positions (2,3). These interactions cause pairwise

covariation between the directly coupled residues, and in the limit of large s we find $C_{AA}^{12} = C_{AA}^{23} = 0.08$, or 8%, but they also cause covariation between the indirectly coupled pair, as $C_{AA}^{13} = 0.04$, or 4%. Furthermore, this Potts model predicts three-body covariation, as can be seen by computing the three-body covariation terms found in cluster expansions in statistical physics given by

$$C_{\alpha\beta\gamma}^{123} = f_{\alpha\beta\gamma}^{123} - f_{\alpha}^1 C_{\beta\gamma}^{23} - f_{\beta}^2 C_{\alpha\gamma}^{13} - f_{\gamma}^3 C_{\alpha\beta}^{12} - f_{\alpha}^1 f_{\beta}^2 f_{\gamma}^3 \quad (2)$$

and we find that $C_{AAA}^{123} = 0.024$, or 2.4%, which is nonzero. This shows that a Potts model generates and can fit higher-order covariation between sets of residues even though the interactions are only pairwise, as a result of indirect covariation through chains and loops of pairwise interactions.

AAA
 ABB
 BAB
 BBA

Table 1. Example MSA following the XOR pattern

An example of MSA triplet statistics which a Potts model is mis-specified to describe is the XOR pattern in which the dataset is composed in equal proportions of copies of the four sequences shown in Table ???. These sequences follow the XOR function in boolean logic, so that the 3rd position is the XOR function applied to the first two positions. One can see that both the A and B residues have a 50% probability at each position, and that for each pair of positions the probability of each of the four combinations AA, AB, BA, BB is 1/4. This means that the pairwise covariances $C_{\alpha\beta}^{ij} = 0.25 - 0.5 \times 0.5$ are all 0. Because there are no pairwise covariances, fitting a Potts model to this data will yield a model with no coupling terms, equivalent to an Indep model. Sequences generated from this (or any) Indep model have all three-body covariation terms equal to 0. However, the three-body covariations of the dataset are non-zero and $C_{AAA}^{123} = 0.125$. This shows how a Potts model fit to XOR data will fail to reproduce the correct three-body covariations. More generally, it will fail to model data which follows a boolean parity function, which generalizes the XOR function to longer strings, and is defined so that the last character is set to "B" if there are an odd number of "B" characters in the preceding sequence.

A motivation for the VAE is that it may potentially be able to model patterns of covariation such as the XOR pattern which a Potts model cannot. Whether a VAE is able to outperform the Potts model when fit to protein sequence data will depend on the prevalence of patterns such as XOR in the data which cannot be fit by a Potts model. If they are undetectable, the Potts model will be well specified and third order parameters are unnecessary. Our results with the natural dataset in the main text suggest no evidence that the Potts model is mis-specified to our dataset, as it is able to reproduce all the MSA statistics we tested up to the limits imposed by estimation and out-of-sample error.

5 Analysis of r_{20} estimation error

When computing the r_{20} scores we are not able to mostly eliminate estimation error, as can be seen by the r_{20} upper limit illustrated in the main text Fig. 2b. Here we provide quantitative intuition for the behavior of the r_{20} score as a function of the evaluation MSA size N which explains why it is difficult to eliminate this estimation error.

Consider a particular set of positions for which we estimate the frequency f of each subsequence at those positions in the target distribution, based on a finite MSA of size N generated from the target distribution, giving estimated marginals \hat{f} . We retain only the top twenty observed subsequences for use in the r_{20} computation. The statistical variance in \hat{f} caused by finite-sampling error will be $f(1-f)/N$, following a multinomial sampling process, and we will approximate that all top 20 marginals have similar magnitude and we approximate this error as $\langle f \rangle (1 - \langle f \rangle) / N$ for all twenty values, where $\langle f \rangle$ is the mean value of the top 20 marginals.

We can then approximate that the expected Pearson correlation ρ^2 between values estimated from two such MSAs will be $\rho^2 \approx \chi^2 / (\chi^2 + \sigma^2)$ where χ^2 is the variance in the values of the top 20 marginals (reflecting the variance of the "signal"), and $\sigma^2 \approx \langle f \rangle (1 - \langle f \rangle) / N$ is the statistical error in each value (representing the variance of the "noise").

$\langle f \rangle$ and χ are properties of the protein family being modelled, at each position-set, and do not depend on N . This invariant allows us to extrapolate, since if we solve for $\langle f \rangle (1 - \langle f \rangle) / \chi^2 = N(1/\rho^2 - 1)$, the rhs should be invariant when we change the size of the dataset MSA from N to N_0 or vice versa. If we estimate the rhs for a particular N_0

and measured ρ_0 numerically, we can solve for ρ at higher N since $N(1/\rho^2 - 1) = N_0(1/\rho_0^2 - 1)$, or

$$N = N_0 \frac{\rho^2/(1-\rho^2)}{\rho_0^2/(1-\rho_0^2)}. \quad (3)$$

The approximations we used to derive this formula will become more accurate for larger N_0 . We have tested this formula by predicting the expected r_{20} for MSAs of size N by extrapolating based on the measured r_{20} for MSAs of smaller size N_0 , and find it is quite accurate.

This equation shows how extremely large MSAs can be required to reduce estimation errors when evaluating r_{20} , as the extrapolated N diverges as $\propto 1/x$ as $x = 1 - \rho^2$ approaches 0. For instance, if with an MSA of 6 million sequences we obtain $r_{20} = 0.8$, then we would require 28.5 million sequence to obtain $r_{20} = 0.95$ and 148 million to reach $r_{20} = 0.99$.

6 Typical natural sequence dataset MSA sizes

The 10K sequence training datasets we use in the main text are meant to illustrate performance for typical protein family dataset sizes. The size of 10K sequences is the number of estimated effective sequences N_{eff} remaining after curation and phylogenetic filtering for the 20th most frequent protein (Cadherin) in Pfam (Fig.5, top).¹³ Some of our measurements show significant out-of-sample error for Mi3 and vVAE based on training sample size alone, suggesting that the vast majority of GPSMs training on natural data could be vulnerable to at least this level out-of-sample error.

In Pfam's Top 20 most frequent protein domains, ranked by total number of sequences, there are between 10^5 and 10^6 total sequences each (Fig.5, right). In this work, we use the 4th most frequent protein out of this ranking, Pkinase. After curation and phylogenetic filtering of the kinase, we retained only $N_{\text{eff}} \sim 22\text{K}$, or $\sim 5\%$ of the original 424K kinase sequences (Fig.5, left). Extending this fraction of $\sim 5\%$ to the other Top 20 proteins, we estimate that N_{eff} is capped at $\sim 10^5$ (100K) for GPSMs trained on single domains, and that proteins outside the Top 20 can generally expect $N_{\text{eff}} < 10^4$ (10K). This simple tabulation of Pfam data demonstrates that, for the vast majority of proteins with publicly available natural sequence data, contemporaneous GPSMs must have approximately $N_{\text{eff}} < 10\text{K}$ for training, validation, and testing.

References

1. Kingma, D. P. & Welling, M. Auto-Encoding Variational Bayes. *arXiv:1312.6114 [cs, stat]* (2014). URL <http://arxiv.org/abs/1312.6114>. ArXiv: 1312.6114.
2. Sinai, S., Kelsic, E., Church, G. M. & Nowak, M. A. Variational auto-encoding of protein sequences. *arXiv:1712.03346 [cs, q-bio]* (2018). ArXiv: 1712.03346.
3. Chollet, F. *et al.* Keras (2015). URL <https://github.com/fchollet/keras>.
4. Kingma, D. P. & Welling, M. An introduction to variational autoencoders. *Foundations and Trends® in Machine Learning* **12**, 307–392 (2019). URL <http://dx.doi.org/10.1561/22000000056>.
5. Ding, X., Zou, Z. & Brooks Iii, C. L. Deciphering protein evolution and fitness landscapes with latent space models. *Nature Communications* **10**, 5644 (2019). Number: 1 Publisher: Nature Publishing Group.
6. Riesselman, A. J., Ingraham, J. B. & Marks, D. S. Deep generative models of genetic variation capture the effects of mutations. *Nature Methods* **15**, 816–822 (2018).
7. Lucas, J., Tucker, G., Grosse, R. & Norouzi, M. Understanding posterior collapse in generative latent variable models. *ICLR 2019 Workshop DeepGenStruct* (2019).
8. Dai, B., Wang, Z. & Wipf, D. The usual suspects? reassessing blame for vae posterior collapse. In *ICML 2020* (2020). URL <https://www.microsoft.com/en-us/research/publication/the-usual-suspects-reassessing-blame-for-vae-posterior-collapse/>.
9. Granata, D. & Carnevale, V. Accurate Estimation of the Intrinsic Dimension Using Graph Distances: Unraveling the Geometric Complexity of Datasets. *Scientific Reports* **6**, 31377 (2016).
10. Schneidman, E., Still, S., Berry, M. J. & Bialek, W. Network information and connected correlations. *Phys. Rev. Lett.* **91**, 238701 (2003). URL <https://link.aps.org/doi/10.1103/PhysRevLett.91.238701>.

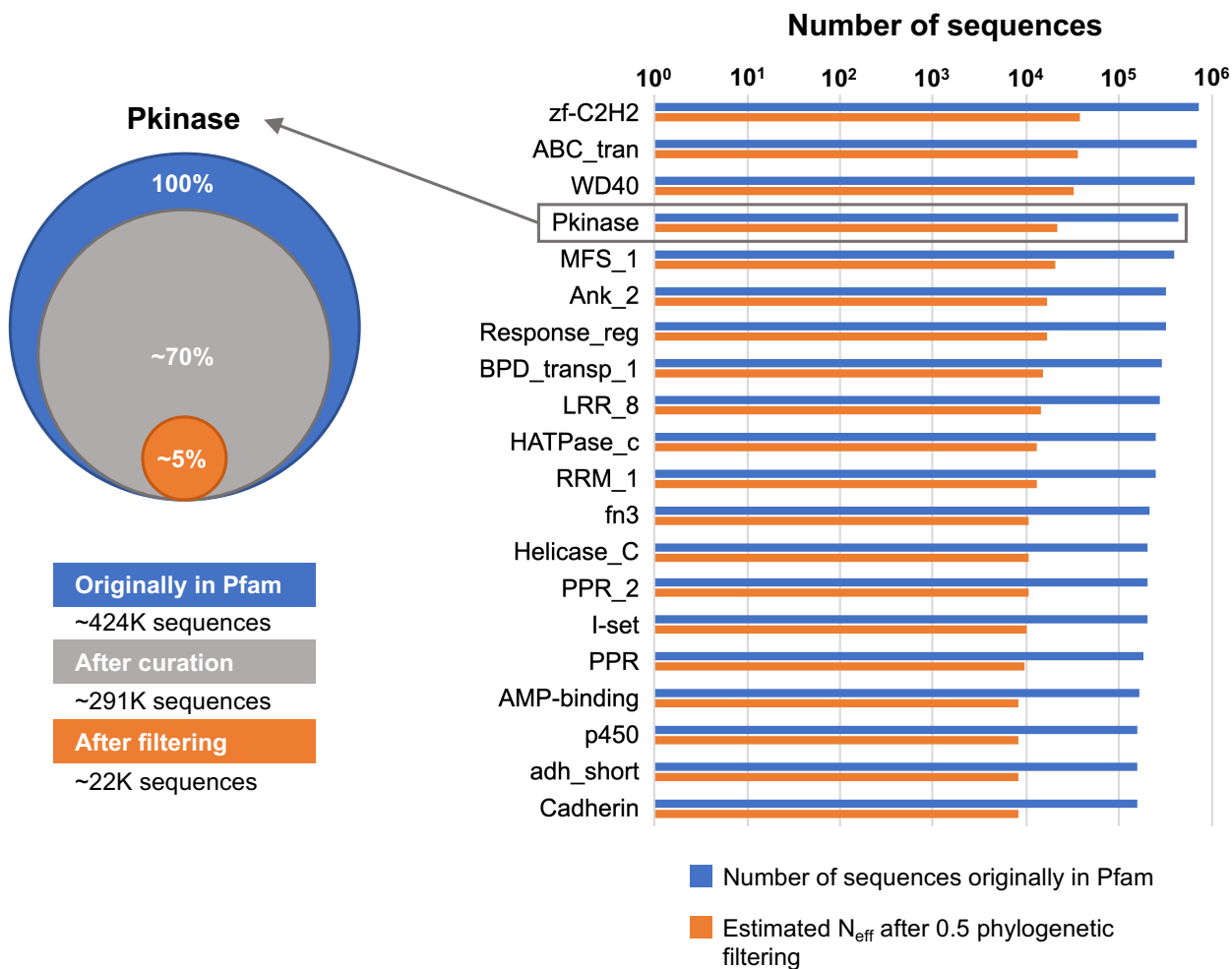


Figure 5. Pfam Top 20. GPSMs trained on publicly available natural sequence data could be inherently data-starved. **Right,** Log-scaled histogram of Pfam sequence frequencies. Sorted by the log-scaled number of sequences originally in Pfam (blue), the histogram shows estimated number of effective sequences N_{eff} after phylogenetic filtering at the 0.5 similarity cutoff (orange). All estimates are based on the actual N_{eff} for Pkinase, the fourth most frequent protein family and the one used in this work, which is ~22K sequences, or ~5% of the total ~424K Pkinase sequences in Pfam (left). Cadherin, the last entry (bottom), has $N_{\text{eff}} < 10^4$ (10K sequences), meaning that this must be the approximate upper-bound of N_{eff} for GPSMs training on natural data outside the Pfam Top 20. Since all proteins outside the Pfam Top 20 must $N_{\text{eff}} < 10^4$, we chose 10K sequences as the lower limit of total training sequences for our synthetic analysis. **Left,** Curation and phylogenetic filtering breakdown for Pfam Pkinase dataset. Of ~424K Pkinase sequences in Pfam (blue), only ~291K (~70%) remained after curation (grey). This curated set was phylogenetically filtered at 0.5 similarity, resulting in $N_{\text{eff}} \sim 22\text{K}$ (orange), or 5% of the original ~424K.

11. Schneidman, E., Berry, M. J., Segev, R. & Bialek, W. Weak pairwise correlations imply strongly correlated network states in a neural population. *Nature* **440**, 1007–1012 (2006).
12. Merchan, L. & Nemenman, I. On the sufficiency of pairwise interactions in maximum entropy models of networks. *Journal of Statistical Physics* **162**, 1294–1308 (2016).
13. El-Gebali, S. *et al.* The Pfam protein families database in 2019. *Nucleic Acids Research* **47**, D427–D432 (2019). Publisher: Oxford Academic.